A full year of continuous net soil and ditch CO_2, CH_4, N_2O fluxes, soil hydrology and meteorology for a drained fen in Denmark

Annelie S. Nielsen[1], Klaus S. Larsen[1], Poul Erik Lærke[2], Andres F. Rodriguez[2], Johannes W.M. Pullens[2], Rasmus J. Petersen[3], Jesper R. Christiansen[1]

[1]Department of Geoscience and Natural Resource Management, University of Copenhagen, Frederiksberg, DK-2000, Denmark
[2]Department of Agroecology, Aarhus University, Tjele, DK-8830, Denmark
[3]Department of Ecoscience, Aarhus University, Aarhus, DK-8000, Denmark

Correspondence to: Jesper R. Christiansen (jrc@ign.ku.dk)

Abstract. We here present a detailed dataset of automated greenhouse gas (GHG) net soil and ditch fluxes of carbon dioxide (CO_2), methane (CH_4), and nitrous oxide (N_2O) from a drained fen in Denmark covering a full year. The dataset resolves small scale spatial and hourly-daily-seasonal dynamics of GHG soil fluxes. The GHG flux dataset is accompanied by simultaneous time series of soil temperature and moisture, as well as groundwater table depth and covers spatiotemporal gradients in soil hydrological and climatic variability. The GHG fluxes of CO_2, CH_4 and N_2O were measured simultaneously by a high-precision cavity ring down laser spectrometer connected with a novel automated GHG system platform called SkyLine2D (Earthbound Scientific Ltd., UK) that allowed up to 27 individual chamber measurement points along a 24 meter transect. In total 47.483 chamber measurements were completed and after quality control 44.631 CO_2 fluxes, 44.099 N_2O and 42.515 CH_4 fluxes remained.

The average (±SE) net soil CO_2 efflux observed at the site (2.6±0.02 µmol CO_2 m^{-2} s^{-1} or 35±0.3 tCO_2 ha^{-1} y^{-1}) aligns with findings from similar drained fens in northern Europe. However, this transect average masks substantial spatial variability and highlights the role of episodic emission bursts related to hydrological variability. The organic soil at the site was a larger net source of N_2O (8.9±0.1 nmol N_2O m^{-2} s^{-1} or 123±1.4 kg N_2O m^{-2} ha^{-1} y^{-1}) to the atmosphere compared to other temperate drained organic grassland soils in northern Europe. The soil N_2O emissions were similarly variable in space as soil CO_2 effluxes, but were more dynamic in time, where increasing groundwater table depth in response to precipitation during warmer seasons led to emission bursts of soil N_2O emissions that dominated the annual net budget of soil N_2O and decreased to near-zero fluxes in drier warmer periods. Net soil CH_4 fluxes were near-zero and the site overall acted as a smaller net source (0.18±0.06 nmol CH_4 m^{-2} s^{-1} or 0.91±0.3 kg CH_4 ha-1 y-1) compared to other drained organic grassland soils, although net uptake of atmospheric CH_4 was observed as well especially in drier conditions.

Diurnal and seasonal patterns of net soil CO_2 and N_2O emissions align with variations of soil temperature, but no clear patterns were observed for net soil CH_4 uptake or emission. Compared to soil GHG fluxes, the ditch was a smaller net source of CO_2 (0.94±0.05 µmol CO_2 m^{-2} s^{-1} or 1.3±0.7 tCO_2 ha^{-1} y^{-1}) and N_2O (0.35±0.03 nmol N_2O m^{-2} s^{-1} or 4.9±0.4 kg N_2O ha^{-1} y^{-1}) to the atmosphere. The ditch was also a net source of CH_4 (161±13 nmol CH_4 m^{-2} s^{-1} or 812±66 kg CH_4 ha^{-1} y^{-1}) average of diffusive and ebullition fluxes) to the atmosphere and annual cumulative emissions were more than two orders of magnitude larger than net the soil CH_4 emissions,

confirming earlier findings that ditches can be CH_4 emission hotspots, where the ditch CH_4 is emitted in bursts with little seasonal variability, including emissions as ebullitions.

The data set (https://doi.org/10.60612/DATADK/BZQ8JE) is well suited for testing and developing biogeochemical models, with emphasis on the soil thermal-hydrology interactions with the peat C and N cycles.

1 Introduction

Understanding the climate feedbacks of temperate drained and rewetted wetlands require robust observational datasets of net fluxes, e.g. whether the rewetted peatlands act as net sources or sinks of greenhouse gases (GHG). This necessitates being able to capture spatial and temporal variability from these systems. Flux data covering all three major GHGs are rare for temperate peatlands, and despite growing efforts to quantify GHG fluxes from drained peatlands, existing datasets often suffer from limited temporal resolution, short monitoring periods, or a lack of concurrent hydrological and meteorological data. Many studies rely on chamber-based measurements or short-term campaigns that fail to capture seasonal dynamics and extreme events. Moreover, current datasets typically offer either high temporal resolution (e.g., eddy covariance or automatic chambers) with poor spatial coverage, or manual measurements with good spatial resolution but very low temporal frequency. In turn this hampers the ability to model and forecast GHG fluxes, and hence climatic feedbacks, in these systems under land use and climatic changes.

However, automated GHG closed chamber flux measurements from ecosystems are becoming increasingly common, also in peatland research (Anthony and Silver 2023; Boonman et al. 2024) as equipment costs decrease and awareness grows about the importance of resolving temporal variability of GHG fluxes to better understand soil biogeochemical processes and soil-climate feedback. But high-frequency data of GHG fluxes are still scarce for peatlands and spatial variability of fluxes is rarely represented as well due to limited number of spatial replicates. Thus, most automated chamber systems are setup around a multiplexer control unit linking multiple chambers with one or more GHG analysers. State-of-the-art automatic chamber systems, like the LI-8250 Automated Gas Flux System (LiCOR, USA) or the eosAC-LT/LO (Eosense Inc. Canada), i.e. allow for a standard number of 8 or 16 chambers, respectively, that can be upgraded to 36 chambers with additional manifolds. Such large replicate chambers allow for improved characterization of spatial variation or treatment effects coupled with temporal variations, but are costly to establish.

Additionally, the introduction of automated chamber systems raises the need for improved data handling and flux calculation tailored to handle a wide range of flux magnitudes and chamber behaviour or design (Kroon et al. 2008; Pihlatie et al. 2013). Recent examples of novel flux calculation software are based on publicly available R codes and include goFlux (Rheault et al. 2024), HMR (Pedersen et al. 2010; Pullens et al. 2023) and fluxfinder (Wilson et al. 2024). Furthermore, unsupervised automated chamber flux measurements increases the likelihood of misinterpretation of fluxes, such as overestimated night-time fluxes due to atmospheric stratification that disturbs the steady-state diffusion gradient between soil and the atmosphere (Brændholt et al. 2017) or leaky chambers that disturb chamber headspace concentrations. This is a significant challenge of automated chamber systems producing thousands of data points, where manual control of each data point may not be practical or feasible calling for automated and objective quality control such as used with the eddy covariance methodology.

We here present a dataset that addresses the abovementioned limitations by uniquely combining high-frequency, continuous measurements of net soil fluxes of carbon dioxide (CO_2), methane (CH_4) and nitrous oxide (N_2O) with detailed hydrological and meteorological variables. The GHG fluxes were measured with an automated GHG chamber system over 12 months resolving spatiotemporal patterns of GHG fluxes including 27 individual collars (26 on organic soil and 1 in a ditch) over a 24 m transect on a temperate drained fen peatland. Integrated

quality control, flagging of erroneous or uncertain flux measurements enabled objective filtering of poor quality data on the entire dataset. This comprehensive spatiotemporal coverage enables robust calibration and validation of biogeochemical and hydrological models, particularly those aiming to simulate the complex interactions between water table dynamics, soil processes, and GHG emissions in managed peatland systems.

Considering the critical need for obtaining high-quality data on soil GHG fluxes from natural and restored peatlands in Europe and globally, our dataset marks an important contribution to this endeavour as it addresses current data shortcomings for Danish and European peatlands by providing detailed data on temporal and spatial patterns of GHG fluxes from organic soils and drainage ditches together with environmental drivers of soil hydrology and temperature, organic soil properties and groundwater geochemistry. We publish this data with the aim of it being used by the scientific community for both experimentalists to test hypothesis of how GHG dynamics are related to hydrology, soil, geochemistry and climate, as well as for the modelers to test and develop biogeochemical models for peat lands.

2 Materials and Methods

2.1 Site description and the SkyLine2D system

The field site, Vejrumbro (N 56.43819 E 9.54527 (WGS 84)), is located in Central Jutland, in Denmark near the city of Viborg (Fig. 1) with a mean annual temperature of 8.3°C and annual precipitation of 675 mm for the period 1991–2020 (measured 6 km away at Aarhus University Viborg Meteorological Station in Foulum (Jørgensen et al. 2023)). It is situated in the Nørre Å valley and is characterized as a riparian fen peat soil (Reza Mashhadi et al. 2024). The riparian fen developed in a former glacial river valley with flat topography gently sloping (<2.5 meters over 300 meters) towards the Nørre Å that forms the central river in this area (Fig. S1). The site was drained in 1950 with ditches and tile drains for cultivation but has primarily served as grassland in recent decades due to the wet conditions (Nielsen et al. 2024). Since 2018, Vejrumbro has been a living lab for agroecological research managed by the Department of Agroecology at Aarhus University. From 2018, the site had a passive rewetting strategy by terminating maintenance of the open ditches. During 2022, the main ditches were gradually blocked.

2.1.1 Site preparation and disturbance

Initially, we chose to perform the flux measurements without aboveground plants as the small chamber dimensions (height of 20 cm) prohibited inclusion of these in the chamber as the plants typically reach over 100 cm in height at this site. The strategy was therefore to focus on measuring net soil GHG fluxes, where we assume the contribution of gases are derived from heterotrophic respiration of older peat C/N, root exudated C/N from adjacent plants, dissolved N in groundwater and belowground autotrophic respiration (CO_2) from roots inhabiting the peat below the collars. We are aware that omitting plants prohibit a full evaluation of the net ecosystem exchange of GHG and hence its net climate impact, as the aboveground plants represent a net sink of atmospheric CO_2 and also can increase the emission of CH_4 and N_2O (Jørgensen et al. 2012; Vroom et al. 2022). However, by avoiding plants we also isolate the soil processes leading to net soil emission/uptake of the GHG and resolve spatiotemporal patterns to a higher degree than previous studies at this site have achieved and what other commercial platforms are capable of. Collectively, this can provide a mechanistic insight into the

regulation of fluxes by hydrology and temperature. We acknowledge that future studies of GHG fluxes in peatlands should seek to include the aboveground plant component to the net GHG flux from the ecosystem.

The disturbance to the transect related to initial harvesting and removal of aboveground plants and continuous removal of aboveground live plant inside the collars and in a small perimeter outside the collar. In this way we kept an approximate area of 40 x 40 cm clear of vegetation at each collar. Two months prior to installation of collars in summer of 2021, the transect (Fig. 2) was harvested and remaining living aboveground vegetation was killed by applying one recommended dose of glyphosate (~100 mg m^{-2}) to the plants only across the transect and avoiding spraying on the soil surface. The half-life of labile glyphosate in mineral soils range between 6-87 days (average 21 days) (Padilla and Selim 2020) with clay contents increasing half-life. The absence of clay and low dosage indicate that there were no, or only little traces of glyphosate left once the flux measurements began and hence the glyphosate treatment likely did not have a direct impact on the measured fluxes. Continued glyphosate application would potentially have reduced microbial activity in the soil and thus lower microbial respiration (Nguyen et al. 2016). Considering that we sprayed the vegetation only one time with glyphosate months prior to flux measurements, we assume the direct impact on soil microbial processes to be small. However, we cannot fully rule out that glyphosate may have led to a transient response. Because we did not have an undisturbed control we cannot quantify the effects of glyphosate. Subsequently, regrowth inside the collars was restricted by manual harvesting of emerging plants at a minimum of once every 7 days and throughout the period. Plant removal from collars is considered a common practice to isolate net soil GHG fluxes as the aboveground autotrophic respiration is removed. Since the individual collars were not trenched it is unavoidable to include belowground autotrophic respiration from plants growing adjacent to the collars. To avoid excessive disturbance of the site we did not remove these roots. Since we did not have a control, untreated/unharvested plot it is not possible to assess the direct impact of the disturbance on the GHG fluxes.

Figure 1: The Vejrumbro location in Jutland (N 56.43819 E 9.54527 (WGS 84)) in the Nørre Å valley near the village of Vejrumbro. The grey circle marks the placement of the SkyLine2D system. Satellite images: © Google Earth.

2.1.2 Peat and organic soil characteristics

In November 2023 the peat across the SkyLine2D transect was sampled to 1 meter depth using a Russian auger and cores split into five layers of 20 cm thickness. Collars 1, 2, 5, 6, 8, 13 – 27 were sampled. For the remaining collars it was not possible to retrieve a sample due to excessive wetness of the peat. The decomposition of the peat samples were assessed by a 10-point Von Post scale of humification (1 = completely undecomposed and 10 = completely decomposed) together with quantification of the pH_{H_2O} (1:5 peat:water mix), dry bulk density (g cm^{-3}) and total C and N by dry combustion (g C/N 100 g $peat^{-1}$ or %) (Table 1).

Table 1 Mean (±standard error of the mean (SE)) peat/organic soil characteristics of humification degree (Von Post), pH (H_2O), dry bulk density (ρ_{dry}), total C (TC) concentration, total N concentration (TN) and the C/N ratio for collars 1, 2, 5, 6, 8 and 13 - 27 at the Vejrumbro transect.

		Von post		pH (H_2O)		ρ_{dry} (g cm^{-3})		TC (%)		TN (%)		C/N	
Depth (cm)	N	Min	Max	Mean	±SE	Mean	±SE	Mean	±SE	Mean	±SE	Mean	±SE
0-20	20	7	10	4.2	0.08	0.31	0.02	26	1.1	1.6	0.06	16	0.4
20-40	20	5	10	4.6	0.06	0.20	0.01	43	1.3	1.8	0.04	24	0.7
40-60	11	3	8	4.9	0.10	0.15	0.01	48	1.8	1.9	0.05	25	1.1
60-80	11	3	6	5.3	0.09	0.11	0.01	47	1.8	1.9	0.05	24	0.6
80-100	10	1	8	5.4	0.09	0.10	0.02	44	2.1	1.9	0.05	24	0.6

153 Generally, there was peat/organic soil to one meter depth except for one collar (25) where gyttja was found in a
154 depth of 80 cm (Table 1). The organic soil was more decomposed in the top 40 cm indicated by higher Von Post
155 values between 5 and 10. Below 40 cm peat still displayed high levels of decomposition along the transect, but
156 was more often found to be less decomposed, values ranging from 1-8 (Table 1). This corresponds well to the
157 previous land use with drainage of the topsoil leading to higher degree of humification. Also, the organic soil
158 was most dense in the top 20 cm (on average 0.31±0.02 g cm^{-3}) and bulk density decreased to 0.10 – 0.12 g cm^{-3}
159 from 40 – 100 cm depth. Total C and N was lowest in the 0-20 cm layer, but still classified as organic soil.
160 Below 20 cm total C and N concentrations, respectively were similar. C/N ratio was lowest in the top 20 cm
161 (16±0.4) and increased to 22-25 in 20 – 100 cm depth (Table 1).

162 2.1.3 Groundwater water sampling and chemical analysis

163 Groundwater was sampled monthly in the piezometers placed at collars 1, 5, 13, 18, 22 and 27 (Fig. 3) by
164 retrieving a 200 mL sample 20-30 cm below the groundwater level at the sampling time. The water sample was
165 retrieved using a syringe and transferred to a plastic bottle that was capped to avoid air bubbles. Water samples
166 were frozen immediately after sampling and subsequently after thawing analyzed for pH, EC and alkalinity on a
167 855 Robotic Titrosampler (Metrohm, Germany). Total N and DOC were measured on a TOC-V CPH Analyzer
168 with Total Nitrogen Unit TNM-1 & ASI-V Autosampler (Shimadzu, Japan). Ion chromatograph (IC) analyses
169 of Cl^-, NO_3^-, and SO_4^{2-} were performed on a 930Compact IC Flex (Metrohm, Germany) and NH_4^+
170 concentrations were measured with continuous flow analysis using a Seal AA500 Autoanalyzer (SEAL
171 Analytic, USA). Total dissolved Fe and P were analyzed with coupled plasma–mass spectrometry (ICP-MS) on
172 an iCAP-Q ICP-MS (Thermo Fisher Scientific, USA) in KED mode using He as the collision gas. Prior to
173 analysis the 10 mL subsamples were acidified with 200 µL concentrated nitric acid to a 10 mL sample.
174 Elemental ICP-MS analyses also included dissolved base cations of Ca^{2+}, Mg^{2+}, K^+, Na^+ as well as total
175 dissolved Al and Mn cations (not shown, but included in the data set).

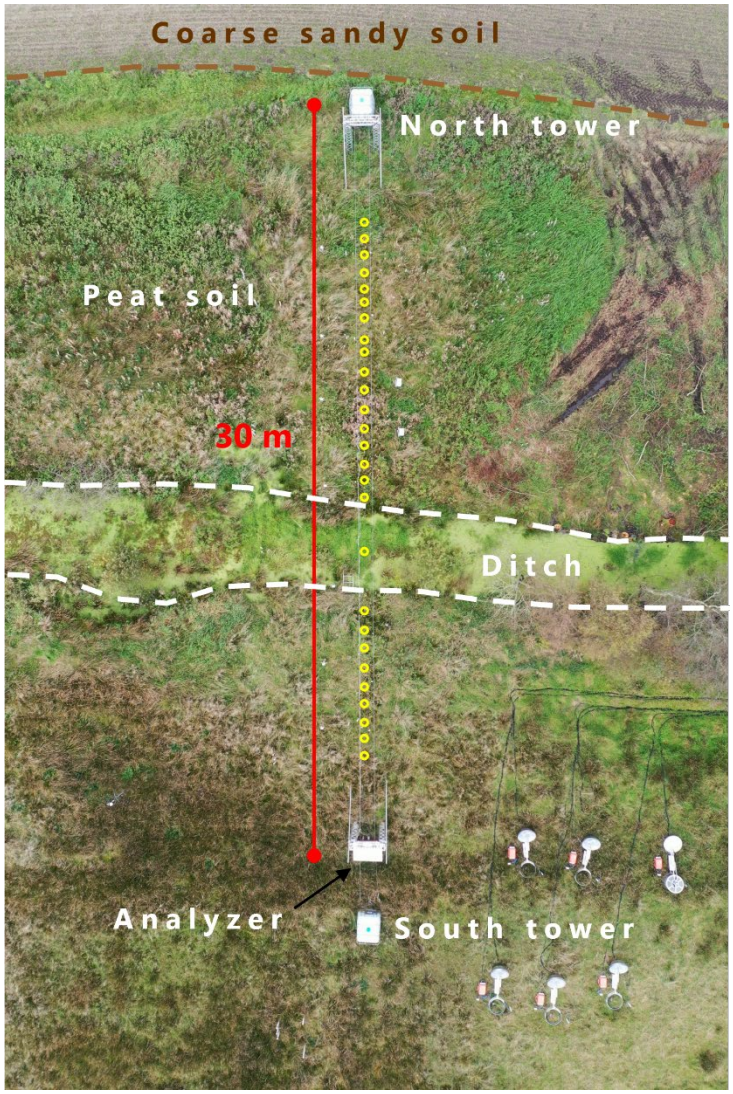

Figure 2: Drone image of the measurement transect (September 27th, 2023) after flux measurements had stopped. Dashed brown line marks the approximate boundary between the agricultural field, coarse sandy soil (north) and the peat/organic soil (south). The red line marks the end points of the SkyLine2D system (30 meters). The open yellow circles (n=27) mark the approximate position of individual collars across the transect of the field (24 meters in length) where greenhouse gas fluxes were measured. The ditch is placed between the dashed white lines. The analyser was placed at the south tower. Elevation above sea level along the 24 meter collar transect varied little from 3.77 m in the south to 4.06 m in the north.

2.1.4 SkyLine2D system configuration at Vejrumbro

The SkyLine2D system is an automated chamber based system for measuring GHG fluxes. The system is designed and built by Earthbound Scientific Ltd. (United Kingdom). We used the SkyLine2D system to measure the net soil fluxes of carbon dioxide (CO_2), methane (CH_4) and nitrous oxide (N_2O) measured with an automated GHG chamber system over 12 months resolving spatiotemporal patterns of GHG fluxes including 27 individual collars (26 on organic soil and 1 in a ditch) over a 24 m transect on a temperate drained fen peatland.

The SkyLine2D system transect was oriented in an north-south direction (Fig. 2). Two 2.5 meter-tall scaffold towers marked the end of the 30 m SkyLine2D system (Fig. 2 and Fig. S2D). The towers were fixed by ropes

attached to 1000L pallet tanks filled with water (Fig. S2D) that maintained a stable position of the towers and ropes and hence placement of the chamber over the collars. The measurement transect was in total 24 m with 27 individual measurement collars for GHG fluxes on the ground, 26 on organic soil and 1 in a drainage ditch (Fig. 2 and 3). The GHG analyser (model G2508, Picarro Inc., USA) was installed in a waterproof and temperature-controlled shelter at the south end of the transect (Fig. 2 and Fig. S2C). The transect was situated on the edge of the riparian fen in close proximity to the mineral upland soils, where active agriculture was practiced (Fig. 2). Along the transect volumetric soil water content (SWC) and soil temperature (ST) as well as water table depth (WTD) were measured at seven locations (Fig. 4). The agricultural field north of the SkyLine2D was sown with annual crops in rotation according to normal practice.

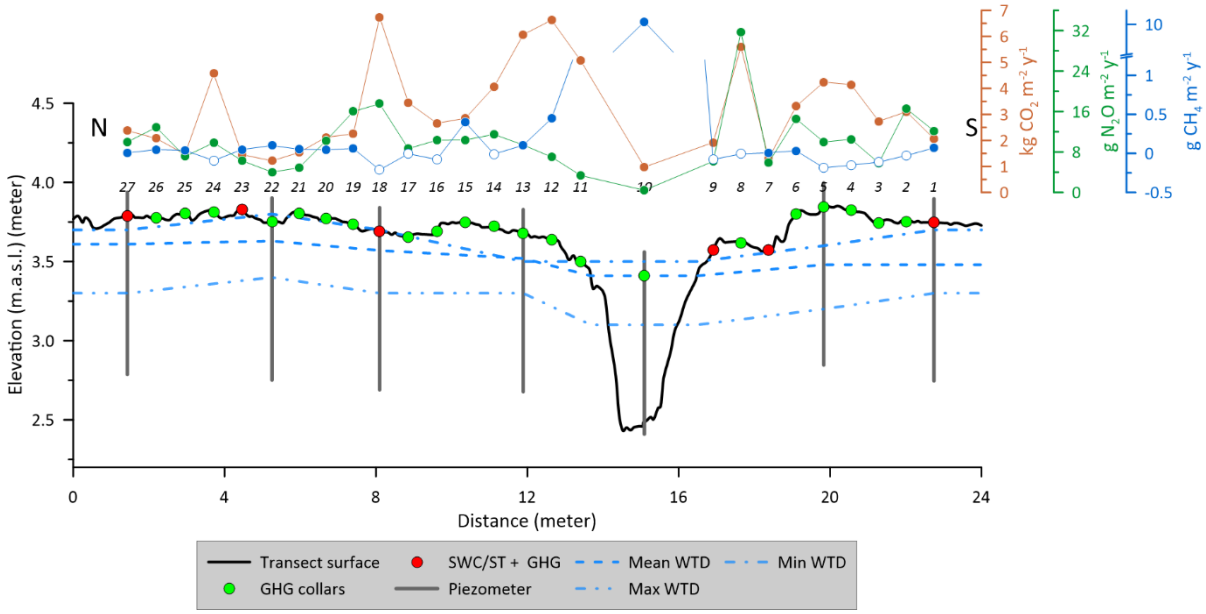

Figure 3: Schematic representation of the measurement transect at Vejrumbro and associated measurement variables. The annual cumulative fluxes of CO_2 (red) (kg CO_2 m^{-2} y^{-1}), N_2O (green) (g N_2O m^{-2} y^{-1}) and CH_4 (blue) (g CH_4 m^{-2} y^{-1}) are shown for each collar across the measurement transect at Vejrumbro. Closed and open symbols for CH_4 represent net cumulative emission and uptake, respectively. Mean WTD is the mean water table depth measured in piezometers (blue dashed line). GHG collars (green symbols) mark the positions of greenhouse gas flux measurements of CO_2, CH_4 and N_2O. SWC/ST + GHG mark the positions where volumetric soil water content (SWC) and soil temperature (ST) at 5 cm depth were measured alongside greenhouse gas fluxes. Numbers on top of plot show the collar numbers (from 1 – 27). N and S mark the north and south ends of the transect (see Fig. 3). The peat depth was at least one meter in all points.

2.2 Overview of time series of GHG fluxes, soil temperature/moisture, air temperature, wind direction and groundwater level

The dataset is comprised of a 12-month time series of net soil fluxes of CO_2, CH_4 and N_2O, accompanied by a longer timeseries of soil temperature and moisture at 5 cm depth, meteorological variables (air temperature, wind speed and direction measured at 2 meter height) and a shorter time series groundwater table level, depth and temperature (Fig. 3, Table 2). Due to equipment failure of the SkyLine2D the GHG flux measurements started on February 2nd, 2022 (Table 2). Groundwater level measurements started between March 9th to 31st, 2022 (Table 1). All other variables were measured continuously from July 1st, 2021, until January 31st, 2023

(Table 1). In the period between December 7th and 19th, 2022 intermittent periods of snow cover (depth was not measured) on the ground occurred. This snow cover did not impede flux measurements.

Table 2: Available time series data from the Vejrumbro SkyLine2D system. Coloured time periods in 2021 to 2023 for each variable indicate data availability.

				Data availability																	
			Frequency (minutes)	2021					2022												2023
Variable	Unit	Model/sensor type		Aug	Sep	Oct	Nov	Dec	Jan	Feb	Mar	Apr	May	Jun	Jul	Aug	Sep	Oct	Nov	Dec	Jan
CO_2 flux*	µmol CO_2 m^{-2} s^{-1}	G2508 (Picarro Inc., USA)	~10**																		
CH_4 flux*	nmol CH_4 m^{-2} s^{-1}	G2508 (Picarro Inc., USA)	~10**																		
N_2O flux*	nmol N_2O m^{-2} s^{-1}	G2508 (Picarro Inc., USA)	~10**																		
Soil temperature at 5 cm depth***	°C	RXW-TMB-868 (Onset, USA)	5																		
Soil water content at 5 cm depth***	(cm^3 cm^{-3})	RXW-SMD-868 (5HS) (Onset, USA)	5																		
Air temperature at 2 m height	°C	S-THC-M002 (Onset, USA)	5																		
Wind speed	m s^{-1}	S-WSB-M003 (Onset, USA)	5																		
Wind direction	°	S-WDA-M003 (Onset, USA)	5																		
Groundwater level****	m.a.s.l.	DCL532 (BD sensors, Germany)	15																		
Groundwater table depth****	cm	DCL532 (BD sensors, Germany)	15																		
Groundwater temperature****	°C	Dallas DS 18B20	15																		

*Net soil/ditch fluxes for all collars 1 - 27.
**Time in between two consecutive flux measurements. The 10 minutes comprise actual flux measurement of 5 minutes and 5 minutes headspace flushing between flux measurements.
***Measured for a subset of collars: 4, 7, 9, 23, 27.
****Measured for a subset of collars: 1, 5, 10 (ditch), 13, 18, 22, 27.

2.3 Soil moisture and temperature measurements

Soil moisture was measured at collars 1, 7, 9, 18, 23, 27 (Figure 4) and probes (6 cm length) were inserted at an approximate 30˚ angle 5 cm outside the collar, while the soil temperature probes were inserted vertically adjacent to the soil moisture probe.

2.4 Groundwater table level and depth

Piezometers (inner diameter 5 cm) were installed at collars 1, 5, 10 (ditch), 13, 18, 22, 27 (Figure 4) to 1 meter depth below the surface, which is deeper than the lowest groundwater level in summer (~60 cm below the surface) with openings from 0.1 – 1.2 meter below terrain. In the ditch the piezometer bottom was deeper than one meter to secure anchoring in the peat. The piezometers were installed approximately 50-60 cm beside the collars to avoid interference with the SkyLine2D system. After installation, piezometers were cleaned and sealed at the surface with bentonite pellets to avoid surface infiltration along the piezometers which can distort water level measurements.

Pressure transducers (Table 2) connected to Arduino-loggers were installed in each piezometer (at collars 1, 5, 10, 13, 18, 22 and 27 – Fig. 3) approximately 1 m below terrain measuring water levels every 15 minutes. The pressure transducers were vented and thus do not need correction for atmospheric pressure.

The groundwater levels were described using two metrics: hydraulic head and groundwater depth (GWD). Hydraulic head represents the water level relative to mean sea level, based on the Danish Vertical Reference (DVR90), while GWD indicates the depth of the groundwater below the surface terrain. The elevation of top of the piezometers were measured using a GPS (model GS07 High Precision GNSS Antenna with a CS20 Controller, Leica, Germany) and used as a local reference for hydraulic head. Manual measurements of groundwater levels were conducted every 2 months and used to calibrate the logger water levels to hydraulic head and GWD.

2.5 Wireless data transfer

Wireless sensors for air temperature, wind speed, wind direction, soil temperature and volumetric soil water content were set up with Wi-Fi data transfer to HOBO RX3000 Weather Station (Onset, USA) equipped with HOBOnet Manager (RXMOD-RXW-868) module for wireless communication with sensors and logged data every 5 minutes. Data access was through the HOBOlink cloud software.

Groundwater loggers were interfaced with the I^2C (Inter-integrated Circuit) protocol and data was collected on Arduino custom-built logger (https://vandstande.dk/logger.php) with wireless connection via LoRaWANor SigFox.

2.6 Greenhouse gas flux measurements with the SkyLine2D system at Vejrumbro

Along the SkyLine2D transect the 26 individual collars (Ø19 cm) along the 24 meter transect on organic soil (Fig. 3) were inserted 5 cm into the peat leaving 5 cm above the surface. The collars were distanced app. 70 cm apart. One collar was installed in the ditch by inserting a tube (Ø19 cm, length 100 cm) to the bottom of the ditch with holes deeper than the minimum water level in the ditch to allow water flow. Thus, it was avoided that

air entered in the collar in the ditch due to low water levels in the ditch. On top of this longer tube a collar (Ø19 cm, length 10 cm) was glued allowing for flux measurements. The chamber was programmed to stop when the bottom of the chamber sat the water surface if the water level in the ditch extended above the top of the collar. For most of the time the collar was not submerged and the chamber therefore hit the collar.

There was one round transparent chamber (height: 39.5 cm and inner Ø: 19 cm, volume: 11.2 L) on the SkyLine2D, hanging below a moving trolley, which was suspended on two ropes stretched between the north and south towers (Fig. S2A and B). At defined positions along the rope, neodymium magnets had been inserted, and a magnet sensor (Fig. S2B) on the trolley informed the internal computer to stop and lower the chamber over positions with a collar on the surface. The chamber was lowered and guided down to the collar by supporting rods shaping a funnel (Fig. S2A). The chamber stopped when it hit the collar, achieved through a pressure sensor on top of the chamber connected to a hollow rubber gasket (Ø 3 cm) at the bottom, which also sealed the chamber with the collar. There was no fan installed in the chamber as the mixing was ensured by the main pump (Fig. S2C). A vent was installed in the top of the chamber to allow for pressure equilibration under windy conditions and chamber deployment.

One entire flux + flushing sequence lasted 10 minutes (Table 1). The chamber closure period was set to 5 minutes with a purging time of 5 minutes in between measurements when chamber was open and hanging underneath the trolley at approximately 1 meter above the ground (Fig. S2D). This provided on average 10 min between flux measurements on consecutive collars (Table 1). Due to small variations in mechanical operations, flux measurements were occasionally farther apart than 10 minutes, but overall, the timing of the SkyLine2D system was consistent. After each cycle of 27 flux measurements there was a 30-minute delay until the start of the next cycle. On average this resulted in 4-5 flux measurements per collar per day throughout the period.

To determine the concentrations of CO_2, CH_4 and N_2O in the chamber air, a laser spectroscopy GHG analyser (model G2508, Picarro Inc., USA) was used. The sample output frequency was set to 1 Hz with a manufactured specified raw precision on 1 Hz data for CO_2: 240 ppb, CH_4: 0.3 ppb and N_2O: 5 ppb at ambient conditions (Picarro Inc., USA). A main pump (model: N86 KN.18, KNF, Germany) circulated the air to and from the chamber at 6 L min^{-1}. The GHG analyser was installed in parallel to the inflow from the chamber due to the much lower flow of 250 mL min^{-1} of the vacuum pump. There was a 30-meter tube between the chamber and main pump to allow for the GHG analyser to remain stationary in the hut while the trolley moved.

2.7 Calculation of diffusive fluxes

Fluxes were calculated and quality checked using the goFlux R package (Rheault et al. 2024) and presented as µmol CO_2 m^{-2} s^{-1}, nmol N_2O m^{-2} s^{-1} and nmol CH_4 m^{-2} s^{-1}. Prior to flux calculations, the gas concentration data from the G2508 was matched to the chamber closure time and chamber id in order to determine the start time of the chamber measurement, so it was possible to separate individual flux measurements from each collar over the measurement time (see examples of flux detection and calculation in Fig. S3A-D). An automatic deadband detection method was applied based on maximal R^2 of a linear regression over the first 180 s (in 10 s steps) after chamber closure. The deadband was allowed to attain values between 0 to 150 seconds thereby also allowing for compensation for the ~60 s delay between chamber headspace gas concentration change and GHG analyser detection due to transport time through the 30 m tube connecting the chamber and GHG analyser.

Flux calculations were done with both linear (LM) and non-linear (Hutchinson-Mosier – HM) regression models (Pihlatie et al. 2013) to determine the slope at time zero. The best flux estimates with either the LM or HM regression model was determined using the *best.flux* function in the goFlux package (Rheault et al. 2024). Shortly, if the RMSE of the HM model was lower than minimum detectable flux (MDF), HM was chosen. However, if the ratio (g-factor) between HM and LM was larger than 2, LM was chosen, as this indicates over-fitting of the HM, which may result in unrealistic large HM flux estimates. If the relative SE of the slope (SE/slope) at time zero for the HM model was larger than 100% it indicated overfitting of the HM model and the LM was chosen. This approach is conservative as it will discard non-linear flux behaviour and instead provide a conservative linear flux estimate. Out of 47.438 detected flux measurements for CO_2, CH_4 and N_2O, respectively, a total of 2807 CO_2 fluxes (5.9%), 3339 N_2O fluxes (7%) and 4923 CH_4 fluxes (10.3%) were discarded either due to chamber mechanical malfunction (imperfect sealing on collar due to erroneous lowering of chamber on collar indicated by background atmospheric or fluctuating gas concentrations in the headspace). At low flux levels non-significant fluxes were discarded as it was not possible to visibly detect whether there was a flux due to high noise-signal ratio of the analyser and/or it was because the chamber had malfunctioned. It is acknowledged that discarding low fluxes can bias annual means and cumulative values, but the data quality did not allow us to determine whether the flux measurement was performed correctly and hence a conservative approach was chosen as including false low fluxes would also bias the data set.

For flux measurements the air temperature in 2 meters was used as an estimate of the chamber headspace temperature along with a 1 atm air pressure.

The annual cumulated fluxes from the soil or the ditch were estimated simply by multiplying the daily average CO_2, CH_4 or N_2O flux for the measurement period with 365 days. We believe for the purpose of data presentation that this simplistic methodology is adequate here, also given the very few data gaps in the timeseries. However, there are other more sophisticated methods using interpolation and response variable functions that may refine the annual budget. However, it is not the goal of this manuscript to present these methodologies but to provide the data so other users can test different temporal upscaling methodologies.

2.8 Calculation of ebullition fluxes in the ditch

Methane ebullition fluxes were occasionally observed only in the ditch. The resultant CH_4 time series for the chamber would have a characteristic appearance (Fig. S4) where the measurement would essentially start out as diffusive flux measurement, then CH_4 bubbles entered the chamber headspace, and the concentration would quickly increase to a maximum value and reach a threshold concentration corresponding to the mixed headspace concentration. In these cases, the LM/HM flux calculation assumptions are violated and instead the ebullition flux would be calculated as the total increase in CH_4 mass m^{-2} per 5 min enclosure. The mass flux of CH_4 per enclosure (nmol m^{-2} per 5 min enclosure) was calculated according to Eq. (1):

$$F_{CH_4-ebu} = dCH_4 * \frac{V_{system}*P}{A*R*T} \quad (1)$$

Where dCH_4 is the concentration difference in nmol between start of chamber enclosure ($CH_{4,start}$) and end CH_4 concentration ($CH_{4,end}$) after it reached a plateau (Fig. S4), V_{system} is the total volume (11.7 L) of the system (collar, chamber, tubes and GHG analyser) in L, P is the pressure (1 atm), A is the area of the collar (0.028 m^2),

R is the gas constant (0.082057 L atm K^{-1} mol^{-1}) and T is the chamber headspace temperature (K). The time step of dCH4 was assumed to be 1 second meaning that the flux unit is nmol CH_4 m^{-2} s^{-1}.

Out of a total of 1728 flux measurements from the ditch (collar 10), 334 were classified as ebullitions indicating that ebullition was erratic which is in line with studies of ebullition of fluxes from ponds (Wik et al. 2016; Sø et al. 2023). Hence, it can be assumed that ebullition occurred around 19.3% of the time during the measurement period (360 days). Furthermore, the ebullition flux is calculated as the accumulated CH_4 in the chamber headspace during the entire flux measurement, e.g. 5 minutes here (Sø et al. 2023), and the calculated ebullition flux in the data set is therefore representative of 5 minute enclosure and not per second. To extrapolate to an annual estimate the number of 5 minute enclosures in 19% of 360 days is therefore estimated (N=20049 5-min 360 $days^{-1}$), multiplied with the average ebullition flux (nmol CH_4 m^{-2} 5 min^{-1}).

Ebullitions could also be caused by mechanical disturbance of the chamber landing on the collar. Ebullition fluxes were discarded if the sudden increase in CH_4 headspace concentration (Fig. S4) occurred 30 seconds after recorded chamber closure as this indicated bubbles released by chamber deployment on top of the collar.

3 Data presentation

3.1 Wind speed and direction

Generally, the wind regime during the measurement period was rather mild with monthly average wind speeds ranging between 1.2 to 2.9 m s^{-1} and maximum gust up to 20 m s^{-1}. The wind direction was uniformly from the west for 52% of the time, with easterly winds constituting 27% and northern and southern winds 8 and 13% of the time (Fig. 4). Winds from western directions were highest for the longest period, while easterly winds were of similar magnitude, but less frequent (Fig. 4). Northern and southerly winds were generally below 3 m s^{-1} and represented periods with still conditions. The very uniform western-eastern wind field at Vejrumbro may also partly be explained by the W-E direction of the valley in which the site is situated, that effectively blocks or dampens winds from S and N.

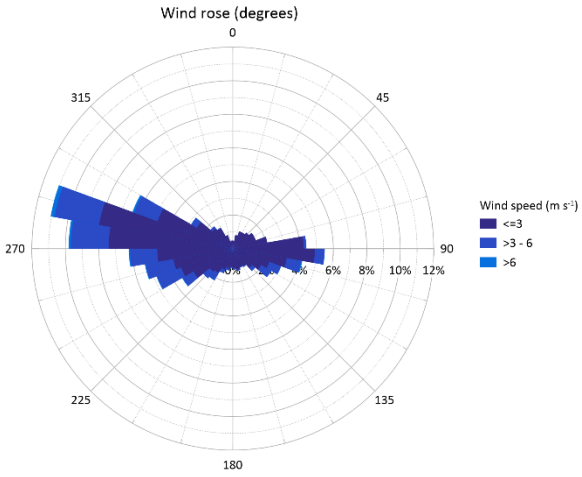

Figure 4: Wind regime at Vejrumbro for the period July 1st, 2021 to January 31st, 2023 presented as a wind rose diagram with wind speed and direction for the period.

3.2 Air and soil temperature

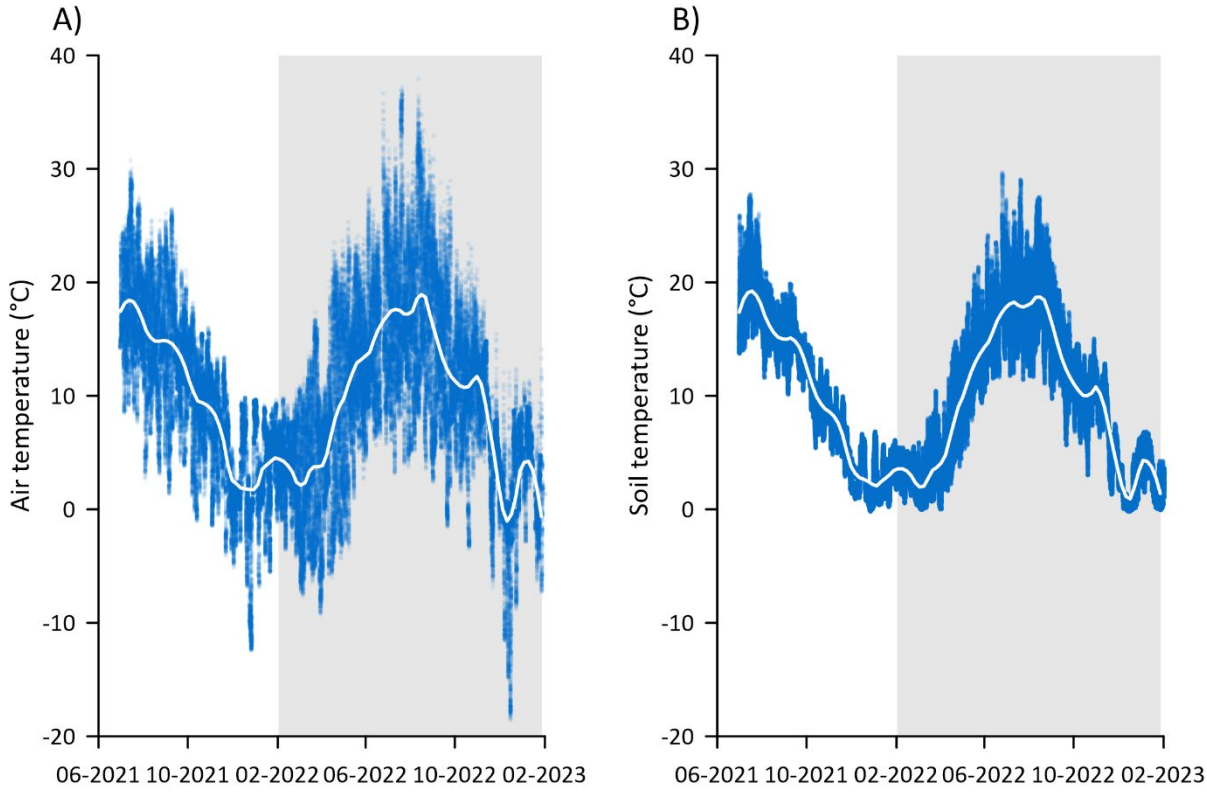

Figure 5: Time series of A) air temperature in °C measured at 2 meter height above the surface and B) soil temperature (°C) at 5 cm depth for collars 4, 7, 9, 23 and 27 along the measurement. The blue dots are the raw 5 min measurements of air temperature and the white lines represent are LOESS fit to show overall seasonal trend. The periods of GHG measurements with the SkyLine2D system are shown with the shaded area.

Over the study period the average air temperature was 9.6°C ranging between maximum 37.9°C and minimum of -18.6°C (Fig. 5A). Monthly ranges of air temperatures (Tab. 2) show >20°C variation between minimum and maximum, except for February, pointing towards large diurnal variations. Soil temperature magnitude and temporal variation were similar across the transect, varying between 0 to 28°C (Fig. 5B) and followed that of air temperature (Fig. 5A) with less variability (Fig. 5B and Table 3). The annual site average soil temperature was similar to the air temperature (Table 3).

374 **Table 3: Monthly mean, maximum and minimum air temperature and soil temperature (°C), groundwater table**
375 **depth (cm) and volumetric soil water content (cm^3 cm^{-3}) at Vejrumbro in the measurement period from February 1st,**
376 **2022 to January 31st, 2023.**

Variable	Year	2022										2023	
	Month	Feb	Mar	Apr	May	Jun	Jul	Aug	Sep	Oct	Nov	Dec	Jan	Avg
Air temperature (°C)	Mean	3.8	3.0	6.6	12.0	15.4	17.7	16.6	13.4	10.7	6.9	1.2	3.7	9.6
	Max	10.6	17.4	23.7	25.3	36.7	37.2	37.9	32.9	23.3	18.4	12.4	14.1	-
	Min	-4.3	-9.3	-8.3	-3.4	4.3	3.2	2.7	-1.5	-3.5	-6.9	-18.6	-7.3	-
Soil temperature (°C)	Mean	3.0	3.2	2.9	6.4	12.3	16.1	18.4	17.0	13.8	10.3	7.2	2.1	9.6
	Max	6.5	5.3	9.1	12.5	18.8	25.1	27.0	24.7	19.3	14.3	12.6	6.3	-
	Min	0.3	1.1	0.4	0.8	6.6	10.7	12.4	11.8	7.0	4.0	2.1	0.0	-
Groundwater table depth (cm)	Mean	-	39	35	41	36	41	35	31	20	18	17	13	29
	Max	-	58	39	58	43	52	46	36	30	31	28	28	-
	Min	-	23	5	24	9	28	22	9	5	6	3	2	-
Volumetric soil water content (cm^3 cm^{-3})	Mean	0.53	0.45	0.40	0.37	0.38	0.43	0.43	0.45	0.50	0.53	0.52	0.51	0.46
	Max	0.56	0.51	0.50	0.41	0.47	0.55	0.56	0.56	0.57	0.58	0.56	0.57	-
	Min	0.43	0.39	0.37	0.33	0.32	0.26	0.32	0.35	0.40	0.47	0.42	0.34	-

377 **3.3 Groundwater table depth**

378 Average groundwater table depth (WTD) below terrain during the period was between 47 to 21 cm across the
379 transect (Fig. 3, Table 3). During summer, the peat drained between 18 – 31 cm below the annual average and in
380 winter the WTD increased to 0 – 22 cm above the annual average across the transect (Fig. 3, Table 3).
381 Generally, the WTD was lower in the ditch across the entire study period (Fig. 3). It was only on the northern
382 end of the transect that the surface occasionally was flooded during winter periods (Fig. 3).

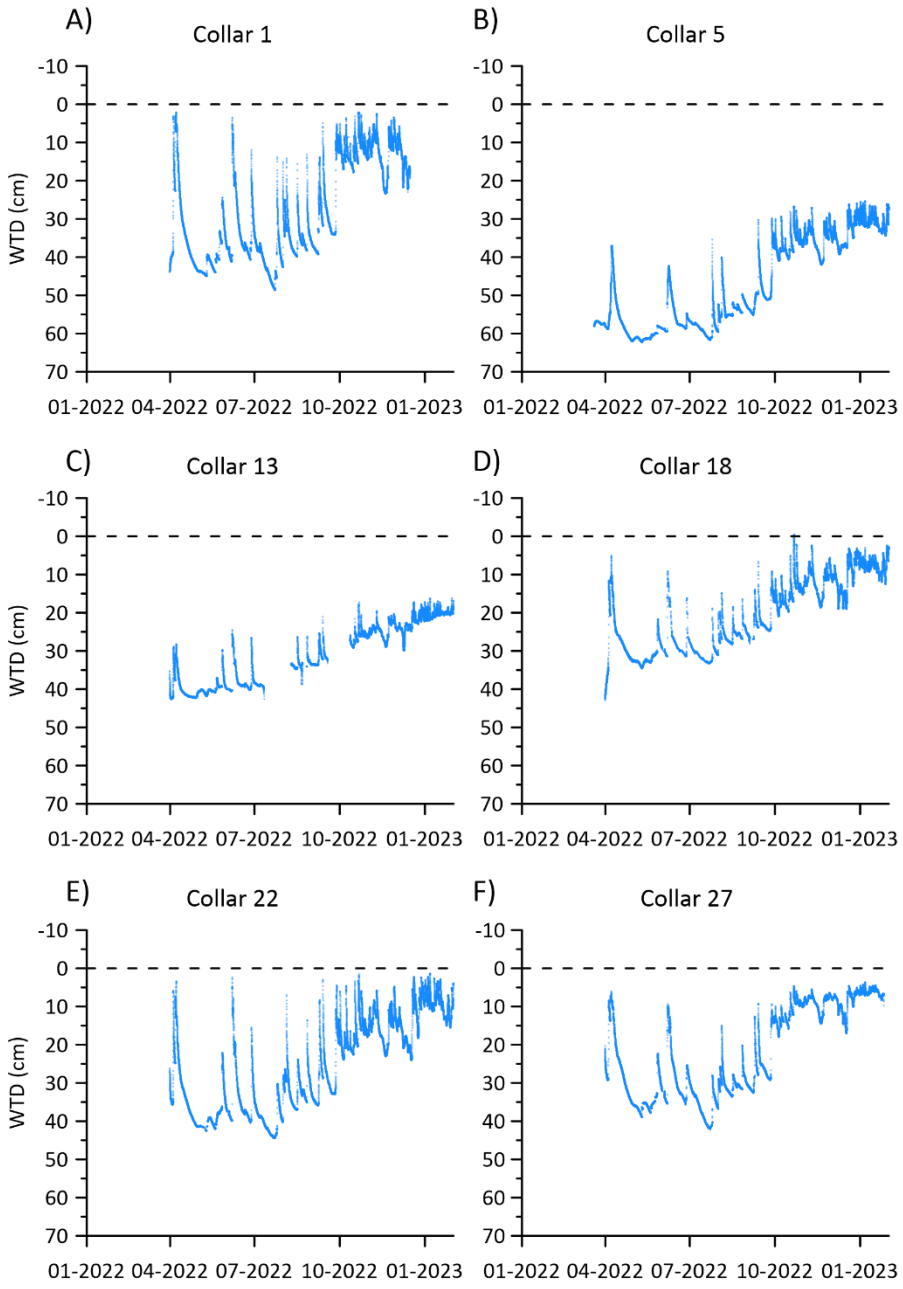

Figure 6: Time series of groundwater table depth (WTD) below terrain for the six piezometer locations along the SkyLine2D transect in the period March 31st, 2022 and January 31st, 2023 when the flux measurements stopped. Dashed line show surface.

The temporal variability of WTD was similar across the transect despite different absolute water table depths (Fig. 6A-F). In the summer periods, the WTD was most variable decreasing to below -40 for collars 1, 13, 18, 22 and 27, whereas the WTD for collar 5 showed the deepest groundwater measured at the site. WTD responded quickly (within hours) to precipitation events that could increase the WTD by almost 40 cm at some plots, indicating that the entire aerated soil volume above the groundwater table was flooded. There was a slight tendency to lower response to precipitation events for piezometers at collar 5 and collar 13 that were placed closer to the ditch (Fig. 3 and 6B and C). As the ditch water level was lower than in the peat this could be explained by more efficient lateral drainage into the ditch from the areas closer to the ditch. In the winter

periods, the WTD was less responsive to precipitation and was closer to the surface (Fig. 6A-F) across the transect.

3.5 Soil water content

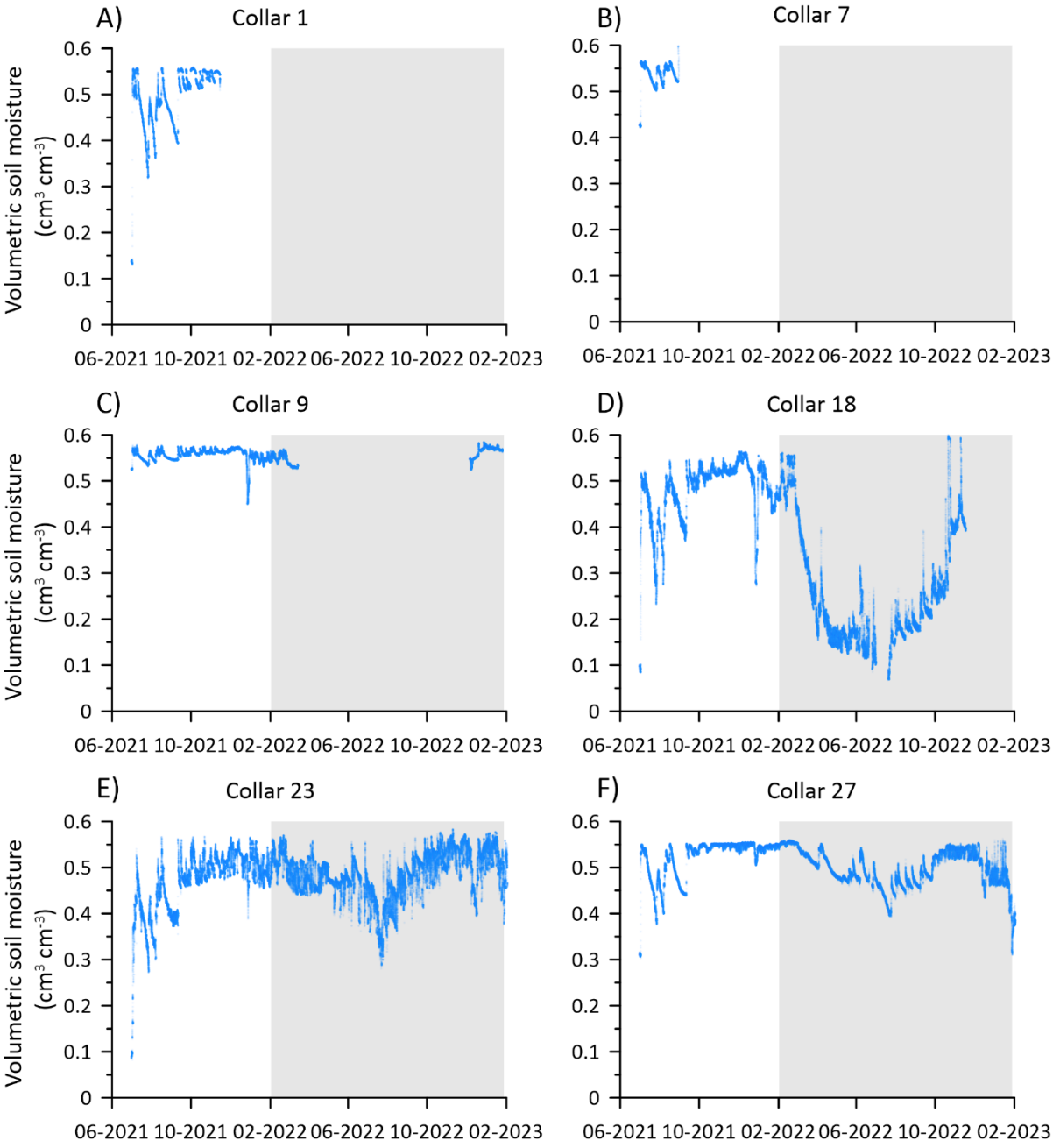

Figure 7: Time series of volumetric soil water content ($cm^3\ cm^{-3}$) in 0-5 cm for the six collars 1, 7, 9, 18, 23 and 27 along the SkyLine2D transect in the period July 1st, 2021 – January 31st, 2023 when the measurements terminated. The periods of GHG measurements with the SkyLine2D system are shown (green lines) on the x-axis.

Due to instrument failure the temporal coverage of soil moisture in the topsoil (5 cm) was not similar across the transect (Fig. 7A-F). For collars 18, 23 and 27 the entire period of greenhouse gas measurements was covered by soil moisture measurements (Fig. 7D-F). While SWC for collars 1, 9, 18, 23 and 27 was similar in the winter periods (around 0.55 $cm^3\ cm^{-3}$) the SWC for collar 18 decreased to lower minima between 0.1 – 0.2 $cm^3\ cm^{-3}$,

than the minima observed between 0.3 – 0.4 cm^3 cm^{-3} for collars 23 and 27 in the summer periods (Fig. 7, Table 3). Similar for all collars it was observed that SWC was more variable in summer, responding similarly as WTD to precipitation events (Fig. 7, Table 3). Since plants were removed regularly from the collars the decrease of SWC for collar 18 cannot be explained by plant transpiration, and the dynamic behaviour could indicate the impact of soil evaporation, but the different levels of SWC also show that there is spatial variation across the transect in the drying properties of the soil. However, it cannot be ruled out that the SWC sensor at collar 18 experienced malfunction or that soil contact was lost in the dry periods of 2022 (Fig. 7D) which could lead to erroneous and too low SWC. Therefore, these data should be considered with care.

3.6 Groundwater and ditch water chemical composition

Site mean pH of the groundwater in the organic soil was 5.8±0.1 and was lower than the pH of the ditch (7.3±0.6). There was a tendency towards lower pH in groundwater and ditch towards the end of the measurement period (Fig. 8A). Electric conductivity was generally higher in the ditch water (359±36 µS cm-1) compared to the groundwater in the organic soil (276±18 µS cm^{-1}) but varied less over the season. The groundwater shows a clear peak in EC around September 2022 (Fig. 8B). Total dissolved P was markedly higher in the groundwater (687±45 µg P L^{-1}) compared to the ditch water (76±10 µg P L^{-1}). Whereas there was little seasonal trend in ditch P concentrations, dissolved P in groundwater dipped to below average concentrations between August to October, likely indicating plant uptake during the growing season (Fig. 8C). Similarly, total dissolved N was higher in groundwater (6.7±0.5 mg N L^{-1}) than in ditch (2.6±1.6 mg N L^{-1}) with increasing concentrations during the growing season (Fig. 8D). Similar, temporal trend was observed for NO_3^- (Fig. 8E), but average groundwater (2±0.5 mg NO_3-N L^{-1}) and ditch (2.2±1.5 mg NO_3-N L^{-1}) concentrations were similar. As expected, dissolved NH4-N was lowest among investigated N-species and there was more dissolved NH4-N present in groundwater (0.8±0.1 mg NH_4-N L^{-1}) than in the ditch (0.14±0.25 mg NH_4-N L^{-1}). However, there was no discernable temporal trend for NH_4^+ (Fig. 8F). Collectively, the temporal trend of TN and NO3- could point to temperature driven mineralization of the peat. Also, the organic N (TN – inorganic N-species) was on average 10 times higher in the groundwater than in the ditch. Average SO_4^{2-} concentrations were similar between the groundwater (17.5±2.4 mg SO_4-S L-1) and ditch (17±1.5 mg SO_4-S L^{-1}), but SO_4^{2-} concentration peaked during September and October in the groundwater whereas it remained more constant in the ditch over the season (Fig. 8G). Similar to dissolved organic N, DOC concentrations were consistently higher in the groundwater (73±3.1 mg DOC L^{-1}) than in the ditch (9.4±3.5 mg DOC L^{-1}), but peaked later in the season, around December 2022, whereas there was little temporal variability of DOC in the ditch (Fig. 8H). Dissolved total Fe displayed the same temporal trend as DOC (Fig. 8I) but was higher groundwater (1916±163 µg Fe L^{-1}) compared to the ditch (98±95 µg Fe L^{-1}). The geochemical parameters of groundwater and ditch water point to different mechanisms regulating especially elements related to peat decomposition and possibly plant uptake, where groundwater was more dynamic over time than ditch water. Generally, there were no systematic spatial pattern of groundwater chemistry across the transect.

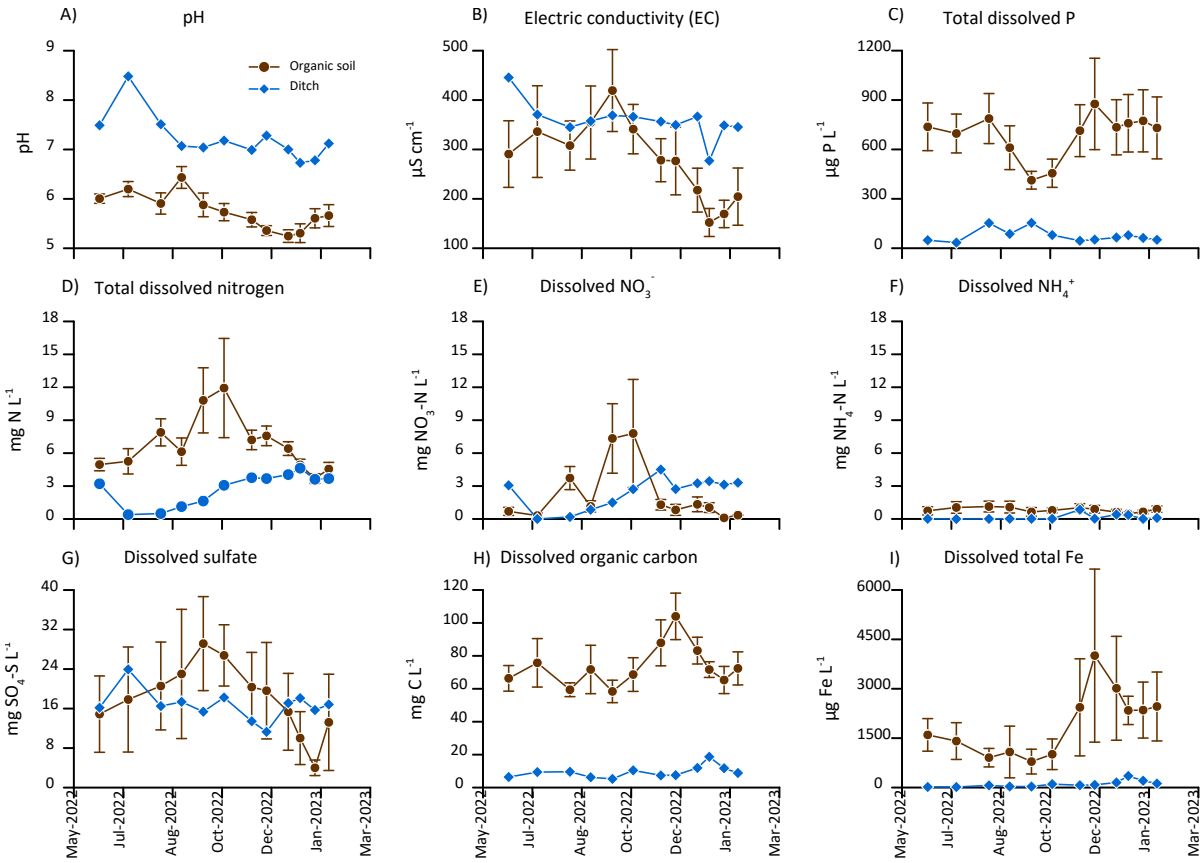

441

442 **Figure 8 Groundwater (brown closed circles) and ditch water (closed blue diamonds) chemistry at Vejrumbro for the**
443 **period June 2022 to February 2023 for A) pH, B) Electric conductivity and dissolved C) total phosphor (P), D) total**
444 **nitrogen (N), E) nitrate (NO_3^-), F) ammonium (NH_4^+), G) sulfate (SO_4^{2-}), H) organic carbon and I) total iron (Fe).**
445 **Values for organic soils are site means with error bars showing the standard error of the mean (N=6 per sampling**
446 **date).**

447 **3.7 Net soil and ditch CO_2, CH_4 and N_2O fluxes**

448 **3.7.1 Spatial variation of net soil CO_2, CH_4 and N_2O fluxes**

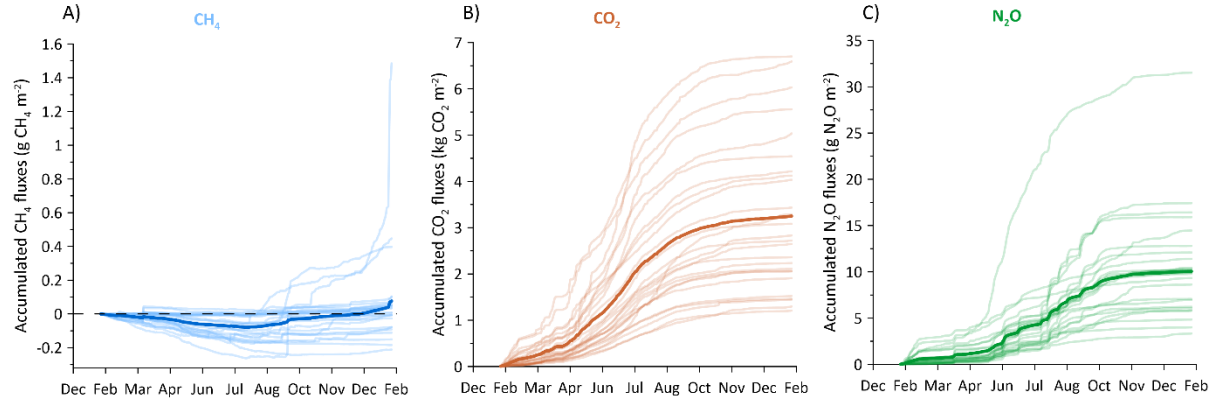

449

450 **Figure 9: Cumulative fluxes of A) CH_4, B) CO_2, and C) N_2O for 26 individual collars along the SkyLine2D transect.**
451 **Units for CH_4 and N_2O are in g CH_4/N_2O m^{-2} and for CO_2 in kg CO_2 m^{-2}. The cumulative fluxes represent the raw**
452 **dataset. The ditch data was excluded. Site average is shown as thick lines.**

Within the transect, cumulative CH_4 fluxes over the study period (360 days) varied between -0.21 to 1.48 g CH_4 m^{-2} over the study period, with a site average (±SE) cumulative flux of 0.07±0.06 g CH_4 m^{-2} (Fig. 3 and 9A). Out of the 26 collars, excluding the ditch collar, 11 displayed a net uptake over the measurement period and the remaining were small net emitters (Fig. 3 and 9A). There was generally little spatial variation in the absolute CH_4 fluxes among the soil collars, but three collars (11, 12 and 15) showed increasing net positive cumulative fluxes towards the ditch (Fig. 3). The low spatial and similar temporal variation between collars indicate both hydrological indicators of SWC and WTD are poor predictors of CH_4 fluxes at this site. However, as we excluded plants from the collars we might have decreased the net emission of CH_4 directly by restricting gas transport in aerenchyma (Askaer et al. 2011; Vroom et al. 2022) and indirectly by potentially reducing plant carbon supply to methanogens. However, visible inspection at the site confirmed lateral root growth from vegetation adjacent to the collar. This could indicate that plant derived C and N was still available for microbes underneath the collars, but the impact on gas transport is uncertain. However, we did not excavate roots during the study to avoid excessive disturbance. Furthermore, considering that the WTD in the growing season was mostly 20-40 cm below terrain the potential for CH_4 production in the topsoil would limited (Koch et al. 2023). Also, the lack of consistent hot moments of CH_4 emissions and low cumulative emissions from the soil despite hydrological conditions in the subsoil being conducive for CH_4 production could indicate that redox potential is elevated due to presence of other electron acceptors. The presence of both free NO_3^-, SO_4^-, Fe (Fig. 8E, G, I) in the groundwater could indicate that there are alternative electron acceptors that prevent lowering of the redox status of the soil and hence suppresses CH_4 production.

The CO_2 effluxes displayed tremendous spatial variation across the 24-meter transect (Fig. 3 and 9B) and measurements indicated that the drained organic soil was a net source of CO_2, with cumulative fluxes over the study period ranging between 1214 – 6740 g CO_2 m^{-2}, and a site average (±SE) of 3269±328 g CO_2 m^{-2}, over the study period of 360 days (Fig. 3 and 9B). There was no apparent relation between the magnitude of cumulative CO_2 efflux to the position along the transect and average WTD (Fig. 3). The cumulative net soil CO_2 emission is equal to 8.9 tCO_2-C ha^{-1} y^{-1} (range of 3.3 to 18 tCO_2-C ha^{-1} y^{-1} across the transect) and compares well to estimates of annual soil C loss (8.8 tCO_2-C ha^{-1} y^{-1}) from a drained unfertilized grassland on organic soil in Denmark (Kandel et al. 2018) as well as annual carbon budgets of similar Danish, British and German wetlands (Tiemeyer et al. 2020; Evans et al. 2021; Koch et al. 2023).

Similarly, the site was overall a net source of N_2O, with cumulative fluxes ranging between 3.3 – 32 g N_2O m^{-2}, with a site average (±SE) of 10.1±1.1 g N_2O m^{-2} (Fig. 3 and 9C) over the study period (360 days). Thus, there is a 10-fold difference between minimum and maximum cumulative N_2O fluxes within the transect, without any apparent relation to the position along the transect and WTD. The highest cumulative N_2O fluxes occurred at collar 8 situated close to the ditch (Fig. 3).The site average cumulative N_2O emission is equivalent to a net N loss from N_2O emission alone of 64 kg N ha^{-1} y^{-1}, was very high and exceeding previously reported fluxes from this site (1.5 – 2.1 g N_2O m^{-2} y^{-1}) (Nielsen et al., 2024) and German organic soils (0.04 – 6.3 g N_2O m^{-2} y^{-1} for grassland and cropland land uses) (Tiemeyer et al. 2020). The high N_2O emission from this site during the measurement period indicate that N_2O may in fact dominate the GWP budget at this site had gross primary production been included in the measurements. It is important to reiterate here that the flux measurements of this study were done on bare soil whereas the studies referenced above included vegetation.

The high N_2O fluxes may be a result of high rates of denitrification in the subsoil from either *in situ* produced NO_3^- from peat decomposition or as NO_3-enriched agricultural runoff from the surrounding intensively cultivated areas, which was not affecting groundwater NO_3^- concentration in the center of the wetland with lower N_2O (Nielsen et al. 2024). The groundwater enters the northern peripheral zone of the wetland at Vejrumbro coinciding with the position of the measurement transect. The highest NO_3^- concentrations in groundwater at the SkyLine2D transect corresponded roughly with highest N_2O emission during summer and early autumn (Fig. 8D-F and Fig. 12D), but the frequency of water sampling was too low to fully link groundwater NO_3^- temporal dynamics to N_2O emissions.

3.7.2 Temporal variability of net soil CO_2, CH_4 and N_2O fluxes

3.7.2.1 Time series of raw data of net soil CO_2, CH_4 and N_2O fluxes

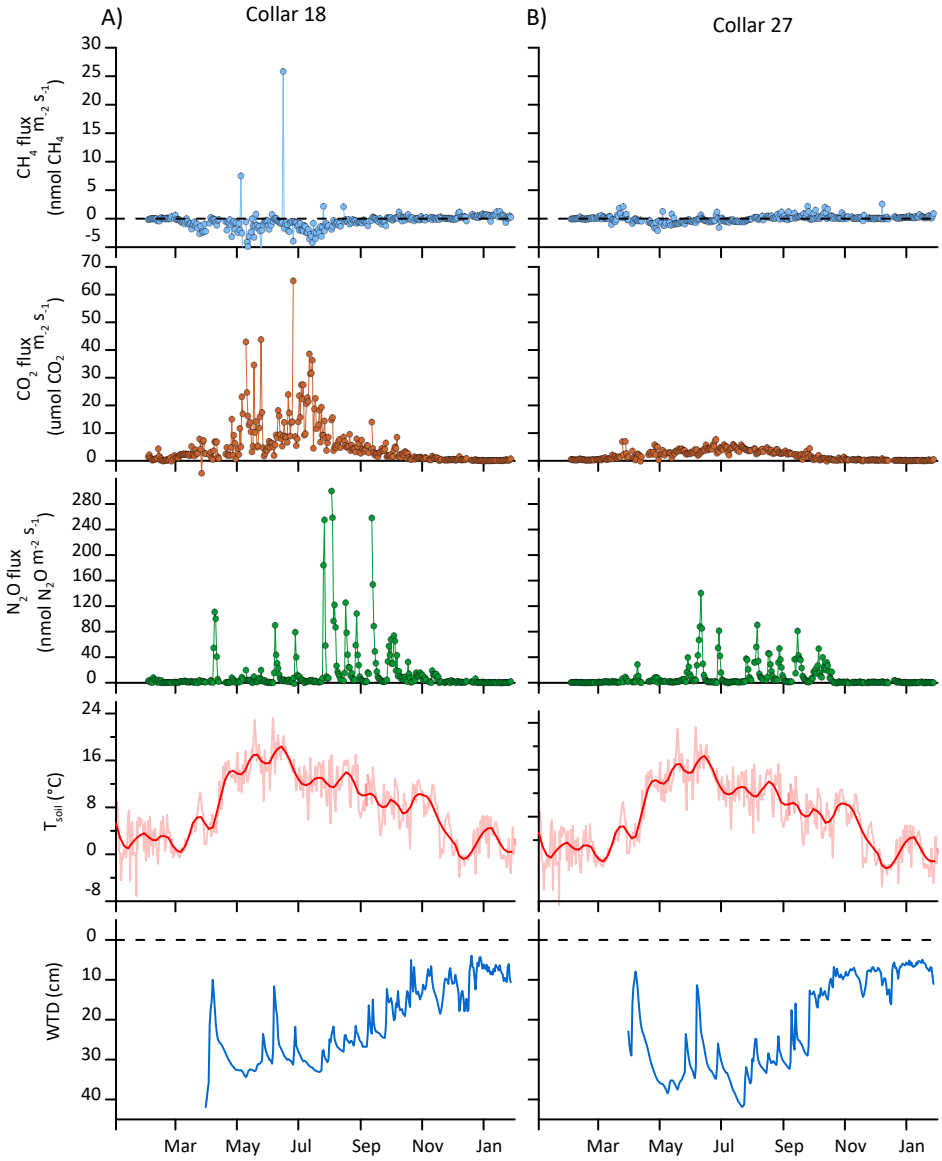

Figure 10: Examples of daily average time series of CH_4, CO_2 and N_2O fluxes for collars 18 and 27 at the SkyLine2D transect in Vejrumbro, soil temperature (ST) in celsius (°C) and groundwater table depth (WTD) in cm below terrain is shown in two lower panels.

With the high frequency of GHG flux measurements (on average 5 measurements per day per collar) it was possible to observe short term flux phenomena that in most studies deploying manual chambers are missed or if captured can lead to biased conclusions on flux magnitudes. For example, in most of the measurement points, CH_4 fluxes were generally near zero, but occasionally displayed elevated net emission for short periods even in periods with deeper WTD (Fig. 10A) for most chambers (see supplementary Fig. S5). This flux dynamic might be related to episodic release of accumulated CH_4 from deeper soil layers that are not fully oxidized in the aerated root zone and that were not released through plants (Askaer et al. 2011). As plants were not included in the collars these bursts cannot be attributed to plant emission pathways.

Generally, it was observed that soil CO_2 fluxes increased over the season with increasing temperature. However, for some collars displayed rapid bursts of CO_2 emissions (example in Fig. 10A), while other collars at the same period did not display this behaviour (Fig. 10B). This dynamic points to different emission pathways from the soil not related to plant mediated transport. Thus, while we purposely omitted aboveground autotrophic respiration by clipping the vegetation, it cannot be ruled out that living roots inhabited the soil below the chambers and hence contributed to the observed CO_2 emission rates.

For N_2O, the spatiotemporal pattern was even more pronounced than for CO2, with N_2O primarily emitted in bursts related to rapidly increasing or decreasing WTD that coincided with precipitation events. In drier periods with deeper WTD and little fluctuations, N_2O fluxes quickly dropped to near zero (Fig. 10A and B). Despite N_2O being emitted in similar temporal patterns across the site, the magnitude of the N_2O peaks were not similar across the transect (Fig. 10 and supplementary Fig. S5). Hence, the majority of N_2O is emitted in hot moments driven by fluctuations in WTD mainly (Fig. 10) as it has also been shown in other drained temperate peatland soils (Anthony and Silver 2023).

3.7.2.2 Diurnal variation of net soil CO_2, CH_4 and N_2O fluxes

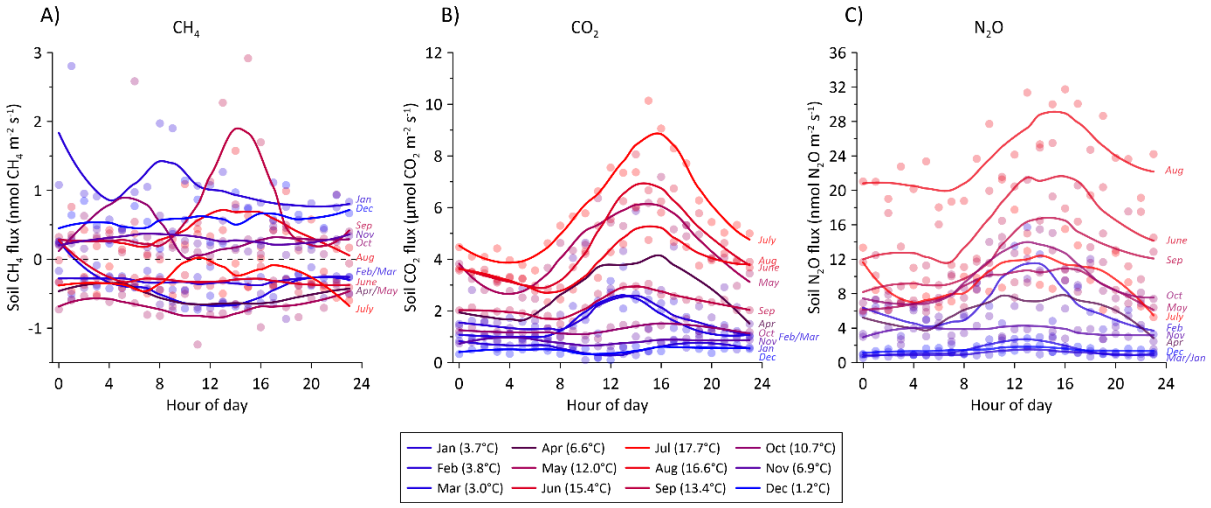

Figure 11: Average hourly flux for all soil collars of A) CH_4, B) CO_2, and C) N_2O during a 24 hour period. The diurnal variation is split between each month during the 2022-2023 measurement period. The fluxes were assigned the hour of measurement during the day and averaged per month. Color shade between blue and red corresponds to average air temperature for the specific month shown in parenthesis in the figure legend. Solid lines are loess fits for visualization of the diurnal variation in each month.

With the SkyLine2D system we observed a clear diurnal cycle for CO_2 and N_2O fluxes, but not for CH_4 (Fig. 11A-C). The lack of diurnal variability of CH4 fluxes could also be due the removal of plants from the collars that would have facilitated light-driven fluxes (Askaer et al. 2011). The amplitude of diurnal variability increased with higher air temperature for CO_2 (Fig. 11B) and partly for N_2O (Fig. 11C). The month of July was an exception as it resembled the pattern observed in May although the July soil temperature was about 5°C higher (Table 2). The lower N_2O fluxes observed in July can be attributed to lower and more constant WTD in July compared to May, June and September across the transect (Fig. 6). Diurnal variability of soil CO_2 fluxes are well known and can be related to both increased heterotrophic respiration during the warmer day and autotrophic respiration in response to photosynthesis. Previously, similar diurnal patterns of N_2O emissions were observed in a Danish fen (Jørgensen et al. 2012).

3.7.2.3 Monthly variability of net soil GHG fluxes

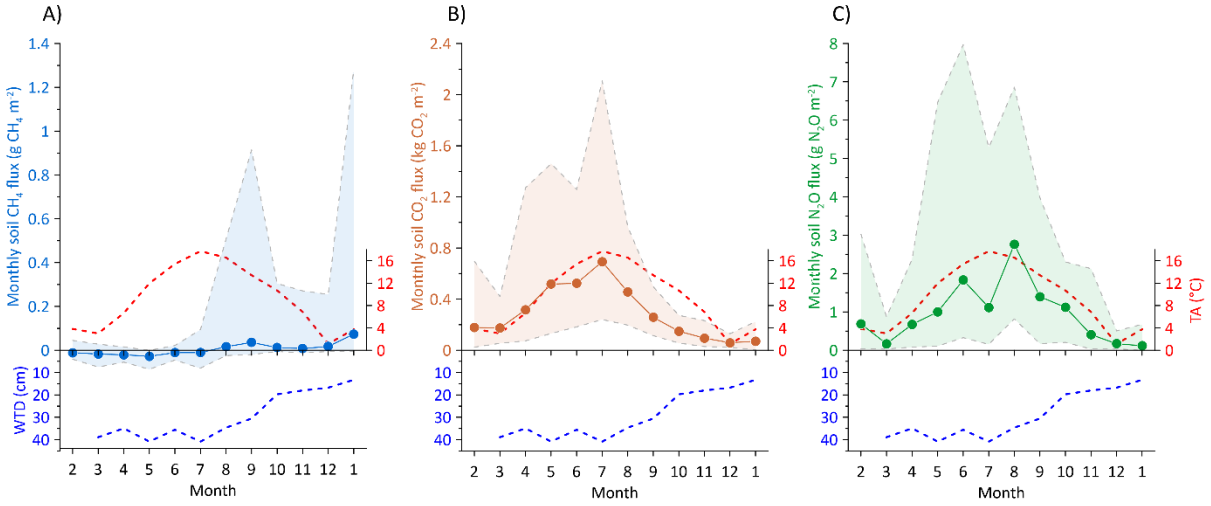

Figure 12: Monthly summed soil fluxes of A) CH_4 in g CH_4 m^{-2}, B) CO_2 in kg CO_2 m^{-2}, and C) N_2O in g N_2O m^{-2} for all organic soil collars. Shaded areas for CH_4, CO_2 and N_2O graphs represent the maximum and minimum monthly average fluxes. Blue dashed line below CH_4, CO_2 and N_2O represent the measured monthly average transect groundwater table depth (WTD) in cm below terrain. Red dashed line shows the monthly average air temperature (TA).

The average soil GHG fluxes for all collars were summed to monthly site sums to illustrate long term drivers on the flux magnitude. Overall, monthly sums of CO_2 and N_2O emissions increase with temperature and fluxes are highest under deeper WTD, but CH_4 net fluxes were less responsive to long term changes in both temperature and hydrology (Fig. 12A-C). Net uptake increased slightly with increasing temperature and lower WTD during the spring and summer. With increasing water table and high temperatures in August the site turned into a small net CH_4 source continuing in fall and winter (Fig. 12A).

For CO_2 the seasonal variation was pronounced and closely followed soil temperature until peak values in July for both site average, minimum and maximum fluxes, respectively (Fig. 12B). From July to August, it was observed that WTD at the site began to increase again and CO_2 fluxes departed from the close relation to soil temperature, indicating an inhibitory role of the WTD in this period, but reaching minimum fluxes in December, corresponding to the wettest and coldest month (Fig. 12B).

Similarly, N_2O fluxes increased with soil temperature reaching peak monthly values in August, corresponding to the period of the year with highest soil temperature and increasing WTD (Fig. 12C). This supports the promoting role of soil water saturation on the production of N_2O when temperature is favourable for denitrification. N_2O fluxes reached minimum values in December when WTD and ST were lowest (Fig. 12C).

3.7.3 Ditch CO_2, CH_4 and N_2O fluxes

3.7.3.1 Time series of raw data of ditch CO_2, CH_4 and N_2O fluxes

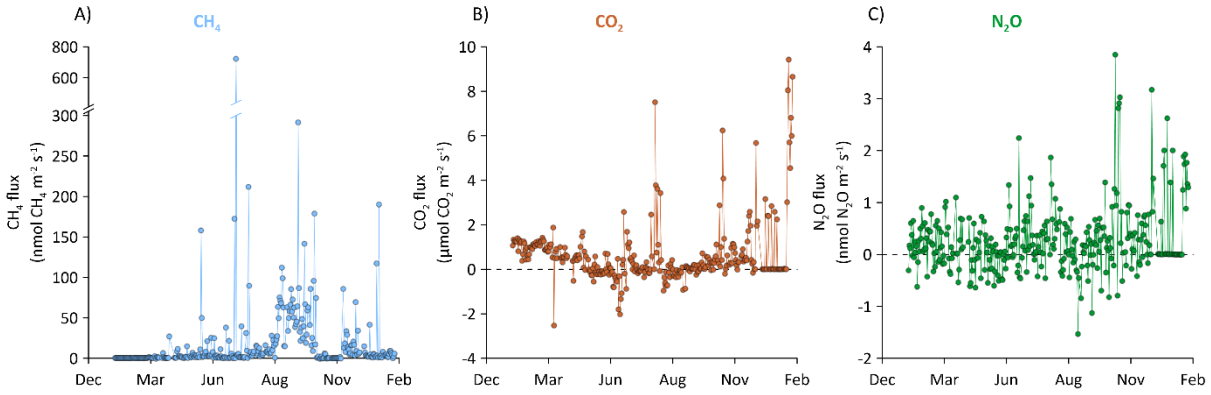

Figure 13: Daily average time series of net ditch total A) CH_4 (diffusion and ebullition), B) CO_2, and C) N_2O fluxes at the Vejrumbro site.

Common for all three gases is that ditch emissions are dynamic and net fluxes change from zero to large net positive or negative fluxes within hours or days (Fig. 13A-C). Compared to net soil CH_4 fluxes the ditch can be considered an emission hotspot at the site (sum of diffusive and ebullition: 8.3 g CH_4 m^{-2} y^{-1}), but fluxes are lower than earlier reports for ditches in other drained wetlands (between 0.1 – 44.3 g CH_4 m^{-2} y^{-1}) (Peacock et al., 2021). Methane is most dynamic with maximum diffusive flux close to 700 nmol CH_4 m^{-2} s^{-1} and there was a tendency toward consistently higher net CH_4 emission from August to September, becoming close to zero in colder seasons (Fig. 13A). Ebullition of CH_4 did occur occasionally in the ditch, e.g. about 19.3% of flux measurements for the ditch was comprised of ebullitions but constituted on average only 2.9% of the total CH_4 emission (0.24 g CH_4 m^{-2} y^{-1}) from the ditch which is lower, but in the same range as a recent estimate from a ditch in a similar drained German peatland (Köhn et al. 2021). According to the flux calculation methodology, flux separation and extrapolation to daily sums, diffusive fluxes dominated (6.56 g CH_4 m^{-2} y^{-1}). However, it cannot be ruled out that the classification as diffusive flux may in fact be ebullition by nature. It has been suggested that microbubbles resulting from mass transport can resemble diffusive fluxes in a chamber making it difficult, if not impossible, to fully separate the two emission mechanisms in a continuous time series if headspace CH_4 concentrations do not abruptly increase (Prairie and del Giorgio 2013), such as in the example shown in Fig. S4.

For CO_2, there was a general tendency towards lower fluxes during the summer months and fluxes increased in magnitude and variability towards the end of the study period (Fig. 13B). For N_2O, the fluxes fluctuated around zero for most of the study period, except towards the end (December and January) where net fluxes became positive (Fig. 13C).

Compared to the net soil N_2O and CO_2 fluxes the ditch fluxes of these gases are low showing that the ditch is not contributing significantly to the CO_2 and N_2O budget at this site.

Per square meter, the ditch emitted less N_2O (0.41 g N_2O m^{-2} or 2.6 kg N_2O-N ha^{-1} y^{-1}) and CO_2 (961 g CO_2 m^{-2} y^{-1} or 2.6 tCO_2-C ha^{-1} y^{-1}) than the organic soil, but was a hotspot of CH_4 emission (8.4 g CH_4 m^{-2} y^{-1} or 63 kg CH_4-C ha^{-1} y^{-1}) during the measurement period. Although these emissions estimates are lower than previously reported for ditches in organic soil (up to 44 g CH_4 m^{-2} y^{-1}) (Peacock et al. 2021). For the ditch CH_4 budget, ebullition only constitutes 2.9% of net CH_4 emissions during the study period. This proportion may be underestimated as the count of ebullition events may have been underestimated (Prairie and del Giorgio 2013).

3.7.3.2 Diurnal variability in ditch fluxes

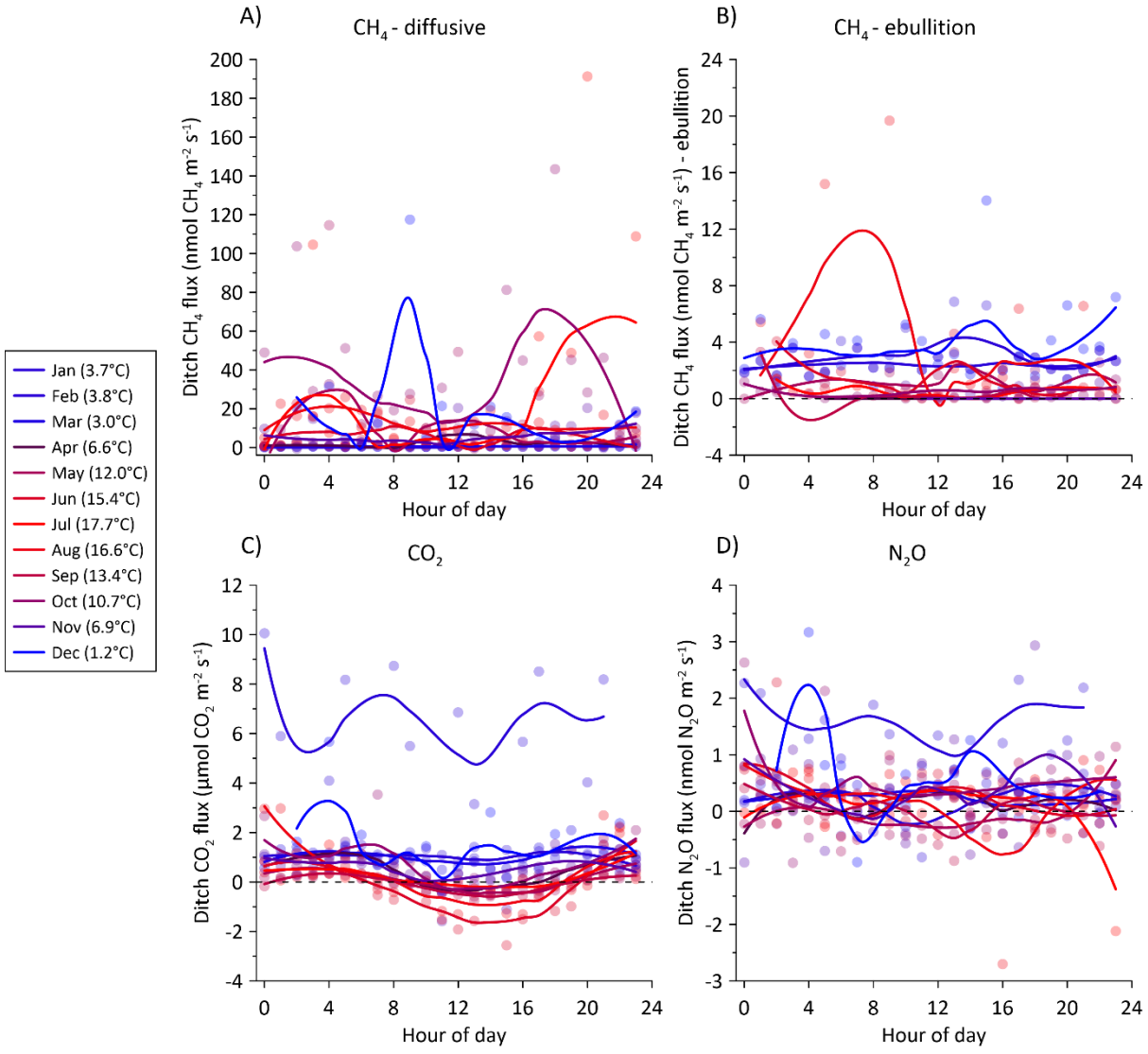

Figure 14: Average hourly fluxes for the ditch collar of A) diffusive CH_4 fluxes, B) CH4 ebullition fluxes, C) CO_2, and C) N_2O during a 24 hour period. The fluxes were assigned the hour of measurement during the day and averaged per month. The diurnal variation is split between each month during the 2022-2023 measurement period. Color shade between blue and red corresponds to average air temperature for the specific month shown in parenthesis in the figure legend. Solid lines are loess fits for visualization of the diurnal variation in each month. Note different axes.

For CH_4 fluxes, both diffusive and ebullition, there was no clear diurnal variability in any month (Fig. 14A and B). This is expected for ebullition emissions which is known to be erratic without any clear diurnality (Wik et al. 2016; Sø et al. 2023). For net CO_2 fluxes from the ditch there was no diurnal variability in colder seasons (Jan, Feb, Mar, Nov and Dec), but consistent positive net CO_2 efflux (Fig. 14C). Diurnal patterns became clearer with higher temperatures from May to October (Fig. 14C) and in this period CO_2 fluxes decreased during the day to sometimes reach net negative fluxes (net uptake of CO_2) during and after midday (Fig. 14C), although the net emissions were also observed in the daytime period (Fig. 14C). The net negative fluxes can likely be explained by photosynthetic activity of aquatic plants on the surface of the ditch or by algae in the water column which was measured due to the transparency of the chamber. Using an opaque chamber instead would likely have resulted in different net CO_2 efflux in daytime. For N_2O, the same pattern as for CH_4 was observed, where flux magnitude across the day fluctuated around zero, except for January where N_2O fluxes were consistently above zero (Fig. 14D).

3.7.3.3 Monthly variability in ditch fluxes

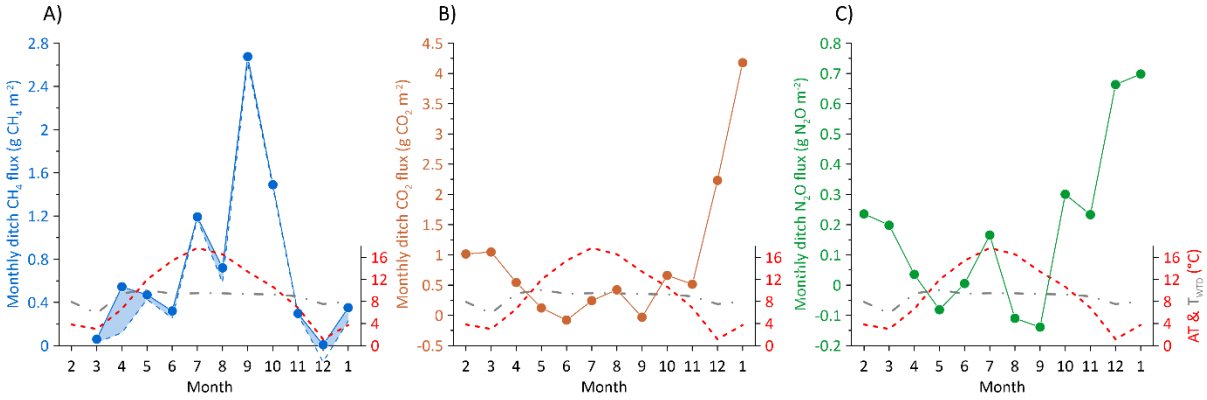

Figure 15: Monthly summed ditch fluxes of A) CH_4 in g CH_4 m^{-2}, B) CO_2 in g CO_2 m^{-2} and C) N_2O in g N_2O m^{-2}. In A) the blue dashed line is the contribution of diffusive fluxes and the shaded blue area between the full and dashed blue lines represent the monthly contribution of ebullition to the total flux. Red and grey dashed lines show the monthly average air (AT) and groundwater temperature (T_{WTD}) in °C, respectively.

The monthly sums of CH_4 tend to increase with air temperature, although peak CH_4 emissions (September) occurred after air temperature peak (July) (Fig. 15A). Diffusive fluxes comprised the major emission pathway of CH_4 in the ditch (between 21% - 99%), with the contribution from ebullition being highest in March (55%) and April (78%) (Fig. 15A). Water temperature in the ditch was relatively stable throughout the year, varying between 5.8 – 10.1°C being highest from April to November and lowest from December to March. However, there is little indication of a direct relation between ditch water temperature and net GHG fluxes (Fig. 15A-C).

For CO_2 and N_2O, the seasonal pattern is reversed with lowest fluxes during the warmest periods, approaching net zero or even net negative fluxes (Fig. 15B and C).

3.7.4 Estimate of the annual soil and ditch GHG budgets at the Vejrumbro location

The annual GHG budgets for N_2O, CO_2 and CH_4 were adjusted from the cumulated values by multiplying with a factor of 365/360. It showed that for the drained organic soil its gaseous carbon loss was mostly as CO_2, while CH_4 played a negligible role in the C cycle and consequently also for global warming potential (GWP) budget.

4 Data availability

Data for this publication is available for download via https://dataverse.deic.dk/previewurl.xhtml?token=abda26d4-a430-4830-ad30-fbf5ff1d352e (Skov Nielsen et al. 2025).

5 Conclusion

The dataset presented here is unique for temperate fens and demonstrate the advantage of using automated GHG measurements systems to resolve temporal and spatial patterns of GHG dynamics in high detail. The dataset also demonstrate how especially temporal variation of soil hydrology and temperature is linked to the dynamics of fluxes and highlight that spatial variability in hydrology and temperatures not necessarily is the best predictor of flux magnitudes within the site. The cause for the spatial variability of GHG fluxes remains unresolved and do not clearly link directly to either WTD, soil temperature and soil/groundwater chemical parameters. Interestingly it appears that the temporal variability of GHG fluxes across the transect is lower than the spatial variation.

The data only represents one full year in 2022-2023 and hence must be considered specific for this period. It must therefore be expected that the annual budget of all GHG's in other years will be different due to other climatic and hydrological conditions.

The initial harvest and herbicide application represent ecosystem disturbances that potentially can alter soil biogeochemistry, but they were done months prior to the start of the flux measurements and hence the direct effect of herbicide would be minimal. The continued plant removal from inside collars was necessary for the flux measurements with the consequence that our fluxes may only be regarded as net soil GHG fluxes, and not as being representative of the net ecosystem exchange. Excluding the influence of vegetation have influenced the measured fluxes of soil respiration (e.g. excluding root exudates etc.) and reduced plant mediated CH_4 and N_2O emissions and lowered most likely also reduced interannual variability. However, the data set represents a unique ability to continue to develop models that predict the soil GHG fluxes in response to soil temperature and hydrology (WTD) that can aid in prediction of reliable budgets for sites.

The measurements of the soil GHG fluxes show that the magnitude of annual cumulative CO_2 fluxes are in the same range as in other studies of temperate fens, and that temporal variability are largely governed by the seasonality of WTD and ST. However, spatial variation of cumulative fluxes for all GHG were not directly related to WTD levels, contradicting the general assumption that WTD is the primary driver of GHG emissions. Cumulative soil N_2O fluxes exceed what has been previously reported for temperate fens, but show similar seasonal regulation by ST. However, in contrast to soil CO_2 fluxes, soil N_2O is emitted largely in pulses related to rapid fluctuations of WTD that increase in size with temperature. These measurements therefore point to an important, but difficult to capture dynamic of N_2O in peatlands where hot moments during the warm periods determine most of the annual emissions. A likely cause for the high soil N_2O emissions could be a combination of leaching of inorganic nitrogen from surrounding agricultural fields and release of organic N from the

decomposing peat. The site was during the measurement period an insignificant source of soil CH_4, which is likely due to the well-drained summer period, a cold wet winter and presence of the major electron acceptors (NO_3^-, SO_4^{2-} and Fe^{3+}), providing suboptimal conditions for CH_4 production. However, it cannot be ruled out that the vegetation removal impeded CH_4 emissions, as we effectively restricted plant mediated CH_4 emissions. Therefore, caution should be taken when comparing the CH_4 flux data to other drained peatlands. Soil CO_2 and N_2O fluxes both showed diurnal variability with higher fluxes during midday where the amplitude between night and day was augmented with ST. This was not observed for soil CH_4 fluxes. The ditch at the site was a net source of both N_2O and CO_2, but at rates 27 and 4 times lower than the soil GHG fluxes respectively. However, the ditch acted as a CH_4 source mostly comprised of diffusive emissions from the water surface, but with observations of ebullition.

We wish to publish this dataset to the research community with the intention that experimentalists and modellers can use the data to test hypothesis on basic hydrological and thermal regulation of GHG fluxes and develop models to predict spatiotemporal variability of the GHG fluxes.

Competing interests

The authors declare that they have no conflict of interest.

Author contributions

JRC, PEL and KSL designed the experiment and carried them out. ASN performed flux calculation and quality checking. RJP and PEL installed the equipment for groundwater measurements. All authors contributed to writing of this manuscript.

Acknowledgements

The measurements are the results of the RePeat (grant nr. 33010-NIFA-19-724), INSURE and ReWet (grant nr. 5229-0002b) projects hosted by University of Copenhagen and Aarhus University. ReWet is part of the Danish roadmap for research infrastructure funded by The Danish Agency for Science and Higher Education. INSURE was part of EJP Soil and received funding from the European Union's Horizon 2020 research and innovation programme under the grant agreement no. 862695.

References

Anthony TL, Silver WL (2023) Hot spots and hot moments of greenhouse gas emissions in agricultural peatlands. Biogeochemistry 167:461–477. https://doi.org/10.1007/s10533-023-01095-y

Askaer L, Elberling B, Friborg T, et al (2011) Plant-mediated CH4 transport and C gas dynamics quantified in-situ in a Phalaris arundinacea-dominant wetland. Plant Soil 343:287–301. https://doi.org/10.1007/s11104-011-0718-x

Boonman J, Buzacott AJ V, van den Berg M, et al (2024) Transparent automated CO2 flux chambers reveal spatial and temporal patterns of net carbon fluxes from managed peatlands. Ecol Indic 164:112121. https://doi.org/https://doi.org/10.1016/j.ecolind.2024.112121

Brændholt A, Steenberg Larsen K, Ibrom A, Pilegaard K (2017) Overestimation of closed-chamber soil CO2 effluxes at low atmospheric turbulence. Biogeosciences 14:1603–1616. https://doi.org/10.5194/bg-14-1603-2017

Evans CD, Peacock M, Baird AJ, et al (2021) Overriding water table control on managed peatland greenhouse gas emissions. Nature 593:548–552. https://doi.org/10.1038/s41586-021-03523-1

Hutchinson GL, Mosier AR (1981) Improved Soil Cover Method for Field Measurement of Nitrous Oxide Fluxes. Soil Science Society of America Journal 45:311. https://doi.org/10.2136/sssaj1981.03615995004500020017x

Jørgensen CJ, Struwe S, Elberling B (2012) Temporal trends in N2O flux dynamics in a Danish wetland - effects of plant-mediated gas transport of N2O and O2 following changes in water level and soil mineral-N availability. Glob Chang Biol 18:210–222. https://doi.org/10.1111/j.1365-2486.2011.02485.x

Jørgensen MS, Plauborg F, Kørup K (2023) Climate normal for Foulum 1991-2020. Aarhus University

Kandel TP, Lærke PE, Elsgaard L (2018) Annual emissions of CO2, CH4 and N2O from a temperate peat bog: Comparison of an undrained and four drained sites under permanent grass and arable crop rotations with cereals and potato. Agric For Meteorol 256–257:470–481. https://doi.org/10.1016/j.agrformet.2018.03.021

Koch J, Elsgaard L, Greve MH, et al (2023) Water-table-driven greenhouse gas emission estimates guide peatland restoration at national scale. Biogeosciences 20:2387–2403. https://doi.org/10.5194/bg-20-2387-2023

Köhn D, Welpelo C, Günther A, Jurasinski G (2021) Drainage Ditches Contribute Considerably to the CH4 Budget of a Drained and a Rewetted Temperate Fen. Wetlands 41:71. https://doi.org/10.1007/s13157-021-01465-y

Kroon PS, Hensen a., Bulk WCM, et al (2008) The importance of reducing the systematic error due to non-linearity in N2O flux measurements by static chambers. Nutr Cycl Agroecosyst 82:175–186. https://doi.org/10.1007/s10705-008-9179-x

Nguyen DB, Rose MT, Rose TJ, et al (2016) Impact of glyphosate on soil microbial biomass and respiration: A meta-analysis. Soil Biol Biochem 92:50–57. https://doi.org/https://doi.org/10.1016/j.soilbio.2015.09.014

Nielsen CK, Liu W, Koppelgaard M, Laerke PE (2024) To Harvest or not to Harvest: Management Intensity did not Affect Greenhouse Gas Balances of Phalaris Arundinacea Paludiculture. Wetlands 44:79. https://doi.org/10.1007/s13157-024-01830-7

Padilla JT, Selim HM (2020) Environmental behavior of glyphosate in soils. Advances in Agronomy 159:1–34. https://doi.org/10.1016/BS.AGRON.2019.07.005

Peacock M, Audet J, Bastviken D, et al (2021) Small artificial waterbodies are widespread and persistent emitters of methane and carbon dioxide. Glob Chang Biol 27:5109–5123. https://doi.org/10.1111/gcb.15762

Pedersen AR, Petersen SO, Schelde K (2010) A comprehensive approach to soil-atmosphere trace-gas flux estimation with static chambers. Eur J Soil Sci 61:888–902. https://doi.org/10.1111/j.1365-2389.2010.01291.x

Pihlatie MK, Christiansen JR, Aaltonen H, et al (2013) Comparison of static chambers to measure CH4 emissions from soils. Agric For Meteorol 171–172:124–136. https://doi.org/10.1016/j.agrformet.2012.11.008

Prairie YT, del Giorgio PA (2013) A new pathway of freshwater methane emissions and the putative importance of microbubbles. Inland Waters 3:311–320. https://doi.org/10.5268/IW-3.3.542

Pullens JWM, Abalos D, Petersen SO, Pedersen AR (2023) Identifying criteria for greenhouse gas flux estimation with automatic and manual chambers: A case study for <scp> N 2 O </scp>. Eur J Soil Sci 74:. https://doi.org/10.1111/ejss.13340

Reza Mashhadi S, Grombacher D, Zak D, et al (2024) Borehole nuclear magnetic resonance as a promising 3D mapping tool in peatland studies. Geoderma 443:116814. https://doi.org/10.1016/j.geoderma.2024.116814

Rheault K, Christiansen JR, Larsen KS (2024) goFlux: A user-friendly way to calculate GHG fluxes yourself, regardless of user experience. J Open Source Softw 9:6393. https://doi.org/10.21105/joss.06393

Sø JS, Sand-Jensen K, Martinsen KT, et al (2023) Methane and carbon dioxide fluxes at high spatiotemporal resolution from a small temperate lake. Science of The Total Environment 878:162895. https://doi.org/10.1016/j.scitotenv.2023.162895

Tiemeyer B, Freibauer A, Borraz EA, et al (2020) A new methodology for organic soils in national greenhouse gas inventories: Data synthesis, derivation and application. Ecol Indic 109:105838. https://doi.org/10.1016/j.ecolind.2019.105838

Vroom RJE, van den Berg M, Pangala SR, et al (2022) Physiological processes affecting methane transport by wetland vegetation – A review. Aquat Bot 182:103547. https://doi.org/https://doi.org/10.1016/j.aquabot.2022.103547

Wik M, Varner RK, Anthony KW, et al (2016) Climate-sensitive northern lakes and ponds are critical components of methane release. Nat Geosci 9:99–105. https://doi.org/10.1038/ngeo2578

Wilson SJ, Bond-Lamberty B, Noyce G, et al (2024) fluxfinder: An R Package for Reproducible Calculation and Initial Processing of Greenhouse Gas Fluxes From Static Chamber Measurements. J Geophys Res Biogeosci 129:. https://doi.org/10.1029/2024JG008208